SIAM J. APPL. MATH.
Vol. 58, No. 1, pp. 142–169, February 1998

008

POPULATION DYNAMICS OF SYNAPTIC RELEASE SITES*

RICHARD BERTRAM† AND ARTHUR SHERMAN‡

Abstract. We describe a mathematical model of synaptic transmitter release that is based on the finding that transmitter release sites and Ca^{2+} ion channels are colocalized in the presynaptic terminal. Because Ca^{2+} channels open and close stochastically, the release model is inherently stochastic. We develop a simple method for representing the collective effect of a population of sites and channels by constructing a system of ordinary differential equations for the mean release. A multiple scale analysis of this system reveals several features of transmitter release and fast facilitation, where release is enhanced if preceded by a conditioning impulse. These include an inverse relation between facilitation and Ca^{2+} cooperativity, a step-like frequency dependence of facilitation, and a release time course that is invariant to changes in the magnitude of release that occurs as the model synapse facilitates or when the external Ca^{2+} concentration is changed. The model is sufficiently simple to be used in conjunction with models of neuronal electrical activity and with neural network models.

Key words. multiple scale analysis, stochastic system, neurotransmitter release model

AMS subject classifications. 92C20, 60K40, 34E10, 60H10

PII. S0036139996297912

1. Introduction.

Neurons communicate primarily through chemical synapses, where electrical impulses called action potentials evoke the release of transmitter molecules. When released, these molecules diffuse across the narrow region separating the presynaptic terminal from the target postsynaptic cell and bind to receptors that are linked either directly or indirectly to ion channels, leading to a local change in polarization of the cell. Transmitter molecules are released through exocytosis, whereby transmitter-filled vesicles fuse with the presynaptic membrane and form pores through which the molecules diffuse down their concentration gradient. Vesicle fusion is thought to occur when Ca^{2+}, brought into the synapse through voltage-gated ion channels opened during an action potential or other presynaptic depolarization, binds to receptor proteins associated with the vesicle and vesicle docking site (see [5] for a review).

Two phenomena, facilitation and cooperativity, have been widely studied. Facilitation is the enhancement of release when preceded by one or more conditioning impulses and represents a form of short-term memory. It is a complex phenomenon that occurs on a number of time scales, but here we treat only fast facilitation on a time scale of tens of milliseconds to a few seconds. Cooperativity is the nonlinear, power law dependence of release on external Ca^{2+} concentration and is thought to reflect the requirement for binding of several Ca^{2+} ions to initiate release at a given site.

Using long trains of impulses, Stanley [21] demonstrated that the cooperativity exponent is four under ideal conditions, low external Ca^{2+} concentration, and low

*Received by the editors February 2, 1996; accepted for publication (in revised form) August 20, 1996.

http://www.siam.org/journals/siap/57-6/29791.html

†Division of Science, Pennsylvania State University, Station Road, Erie, PA 16563 (bertram@euler.bd.psu.edu).

‡Mathematical Research Branch, National Insitute of Diabetes and Digestive and Kidney Diseases, National Institutes of Health, BSA Building, Suite 350, Bethesda, MD 20892 (sherman@helix.nih.gov).

stimulus frequencies ($\sim$ 0.1 Hz). Interestingly, however, he found that as stimulus frequency was increased, cooperativity declined in a step-like fashion, approaching one at $\sim$ 100 Hz. At the same time, facilitation increased in a step-like fashion. This reciprocal relation between cooperativity and facilitation led Stanley to hypothesize that each release site contains four Ca^{2+} binding sites or gates, each of which must be bound for release to occur, with unbinding kinetics graded from slow to fast, and affinities ranging from high to low. The downward steps in cooperativity then reflect the progressive saturation of faster gates as frequency increases, and the corresponding upward steps in facilitation reflect the ability of faster gates to retain their bound Ca^{2+} between pulses as the interpulse interval decreases.

Figure 2.1 illustrates how the probability of release at a site increases in the second impulse because some of the Ca^{2+} bound during the conditioning impulse is still bound. The three observed steps in facilitation suggest that three of the four gates per release site have slow unbinding kinetics, ranging from moderately slow (tens of milliseconds) to very slow (seconds). The remaining gate is fast, so that release from the synaptic terminal terminates almost immediately after the end of the action potential, another characteristic feature of synaptic release. This "residual bound Ca^{2+} hypothesis" stands in contrast to an alternate hypothesis that facilitation is due to an elevation of free Ca^{2+} left over from the conditioning impulse [24], [26].

Transmitter release occurs within 200 μsec of the opening of Ca^{2+} channels, suggesting that vesicle release sites and Ca^{2+} channels are separated by a distance of no more than 100 nm [16]. Other studies have shown that release can be evoked by the opening of a single Ca^{2+} channel, placing the release site close enough to the channel so as to be activated by the microdomain of Ca^{2+} surrounding the channel's mouth [2], [22], [25]. Action potentials are typically 1 to 3 msec in duration. The low Ca^{2+} channel opening probability per unit time makes it unlikely that adjacent channels will be open simultaneously during such short depolarizations; thus most of the release of transmitter will be from vesicles activated by Ca^{2+} in single-channel microdomains. Stanley [22] proposed that transmitter release sites are colocalized with Ca^{2+} channels.

We have translated Stanley's verbal model into a mathematical one [4]. We assumed that each release site is associated with a single channel, allowing us to neglect the dynamics of Ca^{2+} diffusion between channels. Although this is likely an oversimplification, we were able to show that the model captures many of the key features of transmitter release. In particular it shows that facilitation can occur without accumulation of residual free $Ca^{2+}$and it exhibits steps in facilitation and cooperativity.

However, the colocalization assumption introduces a new complication: the release sites inherit the stochasticity of Ca^{2+} channel opening, which is averaged out by diffusion in other models. We therefore employed two models in our first study, a deterministic caricature, in which the gates are driven by Ca^{2+} pulses, and a stochastic model, capable of simulating action-potential- or voltage-clamp-driven release. The simplicity of the deterministic model enabled us to derive analytic expressions for release and facilitation and to analyze the effects of varying physical parameters. We showed for a limiting case that although release increases with external Ca^{2+} concentration, facilitation decreases, in agreement with experiments [19], [21].

By focusing on channel dynamics, the stochastic model permitted study of a phenomenon that hitherto had been treated in an artificial way. The bulk of release occurs not during depolarization but in the tail following repolarization, when the

product of channel open probability and domain Ca^{2+} is maximized (see Fig. 2.4). It also reproduces the almost complete invariance of the release time course as release magnitude increases via facilitation or increased external Ca^{2+} concentration [6]. This has been problematic for at least one transmitter release model [26].

In [4], the stochastic model was solved using a Monte Carlo method to simulate channel openings and closing. This is cumbersome and very time consuming computationally, too slow, for example, to demonstrate steps in facilitation. It is also difficult to analyze. Although invariance of the release time course was demonstrated, the simulations did not explain *why* the time course is invariant. Here we derive a system of ordinary differential equations that describe the mean behavior of the population of sites and channels without direct Monte Carlo simulation. This method is not only much easier to use in simulations, it is also more amenable to analysis.

In section 2 of the present paper we first review the deterministic and stochastic models. Then we reformulate the stochastic problem as a system of hyperbolic conservation laws for the probability distributions (Figs. 2.2, 2.3) and use this to derive the equations for the expected value of release. In section 3 we show that the mean release for the stochastic model exhibits frequency-dependent steps (Fig. 3.1) similar to those shown previously for the deterministic model [4].

In section 4 we carry out a multiple scale analysis of the mean release system. In section 4.1 the facilitation process is analyzed in terms of the time course of each of the slow gates. For a slow gate, it is shown that during a train of impulses the average bound concentration rises exponentially on a slow time scale, with a time constant that depends on the Ca^{2+} unbinding rate (Fig. 4.1A). In section 4.2 we analyze the step-like frequency dependence curve and derive a leading order approximation curve (Fig. 4.2). The analysis in section 4.3 shows why the model has the invariance property described above (Fig. 4.1B,C). It also shows that invariance persists over a long train of impulses, even though the degree of facilitation is different for different external Ca^{2+} concentrations. Finally, in section 4.4 we analyze the decrease in Ca^{2+} cooperativity with facilitation.

Although the system describing mean release is much simpler to use than a Monte Carlo simulation, it is still prohibitively large (30 differential equations) for many applications. Motivated by the multiple scale analysis, we show in section 5 that it is not necessary to know the detailed distribution of open Ca^{2+} channels to compute the time course of the mean bound concentration of a slow gate; it is well approximated by the mean-field representation using only the ensemble average of the domain Ca^{2+} concentrations (Fig. 5.1). With this approximation, release requires only three equations. This and other suggested reduced forms make the model sufficiently simple for use with both single neuron models and neural network models (see [3]).

2. Deterministic and stochastic models.

2.1. Deterministic model of calcium binding and release. Each release site is assumed to contain a Ca^{2+} channel and four independent Ca^{2+} binding sites or gates. The binding of Ca^{2+} to the jth gate has first-order kinetics

$$U_j \underset{k_j^-}{\overset{k_j^+ Ca}{\rightleftharpoons}} B_j\,, \quad j = 1,2,3,4, \tag{2.1}$$

where U_j and B_j are the nondimensional concentrations of unbound and bound gates, repectively, whose sum is normalized to 1 (they may also be viewed as probabilities).

Ca is the domain Ca^{2+} concentration which we assume to be proportional to the influx through a single Ca^{2+} channel. (We also assume that this influx is proportional to the external Ca^{2+} concentration.) Binding rates (k_j^+, in $\text{msec}^{-1}\mu\text{M}^{-1}$) and unbinding rates ($k_j^-$, in msec^{-1}) are $k_1^+ = 3.75 \times 10^{-3}$, $k_1^- = 4 \times 10^{-4}$, $k_2^+ = 2.5 \times 10^{-3}$, $k_2^- = 1 \times 10^{-3}$, $k_3^+ = 5 \times 10^{-4}$, $k_3^- = 0.1$, $k_4^+ = 7.5 \times 10^{-3}$, $k_4^- = 10$. The k_j^- vary from small to large, while the k_j^+ are small for all gates. We will carry out different perturbation analyses below, depending on whether k_j^+ and k_j^- are both small or only k_j^+ is small. The dissociation constants ($\kappa_j = k_j^-/k_j^+$) for gates S_1 through S_4 are 108 nM, 400 nM, 200 μM, and 1334 μM, respectively. Thus, the Ca^{2+} affinities ($1/\kappa_j$) of the gates are graded from high (9 μM^{-1} for S_1) to low (7×10^{-4} μM^{-1} for S_4). Unbinding time constants ($1/k_j^-$) are 2.5 sec, 1 sec, 10 msec, and 0.1 msec, respectively.

The probability that the jth gate is bound evolves in time according to the differential equation

$$\frac{dB_j}{dt} = k_j^+ \, Ca(V) - (k_j^+ \, Ca(V) + k_j^-) \, B_j \, , \quad j = 1,2,3,4. \tag{2.2}$$

If the associated Ca^{2+} channel is closed then $Ca = 0$, otherwise it is a function of the membrane potential (V), which is time dependent. Therefore, Ca provides time-dependent forcing to the system. The release site is activated when all four gates are bound; thus the probability of release per unit time (or the rate of release) is

$$R = B_1 \, B_2 \, B_3 \, B_4. \tag{2.3}$$

This model is deterministic provided that the opening and closing of the associated Ca^{2+} channel, and thus Ca, is deterministic, which we assume to be the case for now.

Release from a single site is facilitated during the second of two impulses if the probability of release during this impulse is greater than that during the first impulse (facilitation of a population of release sites is defined as the ratio of release evoked by the impulses). This process is illustrated in Fig. 2.1. Prior to the first impulse there is no Ca^{2+} bound to any of the four gates (not shown). With the first impulse the associated Ca^{2+} channel opens, letting in Ca^{2+} which binds to three of the four gates, but because S_3 remains unbound there is no release. Almost immediately upon channel closure Ca^{2+} unbinds from S_4, which has a fast unbinding rate. Ca^{2+} remains bound to S_1 and S_2 for hundreds to thousands of msec since the unbinding rates of these gates are low, so if the second impulse occurs within this time interval Ca^{2+} must bind to only two gates to induce fusion of the vesicle and the release of transmitter.

A crucial feature of this scheme is the wide variation of Ca^{2+} unbinding rates among the gates. The high Ca^{2+} unbinding rate of S_4 ensures that release terminates quickly upon channel closure, consistent with the experimentally observed fast time course of release following a stimulating impulse. The three distinct unbinding rates of the other gates provide three components of facilitation. Low frequency trains of stimuli (less than 0.5 Hz) facilitate release only through the slowest gate, S_1. Stimulus trains with higher frequencies up to 20 Hz facilitate through S_1 and S_2 but not S_3. Trains with frequencies above 20 Hz facilitate through all three slow gates. Using a stimulus protocol in which Ca is a fixed positive constant during each stimulus and zero between stimuli, we showed [4] that this leads to a facilitation curve that increases in a step-like manner with increasing stimulus frequency. Due to the simple

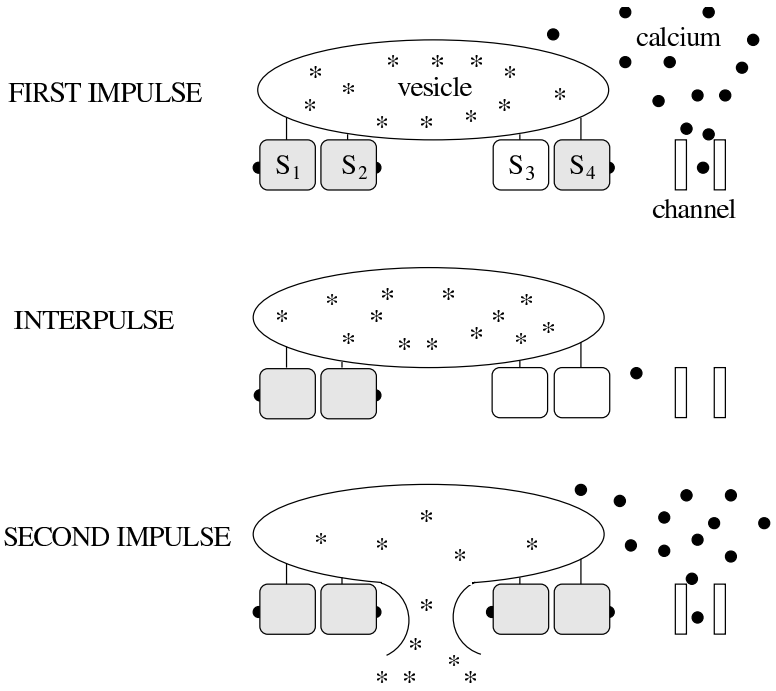

FIG. 2.1. *Illustration of the single domain/bound calcium hypothesis for transmitter release and facilitation. The release site complex consists of a transmitter-filled vesicle, fusion machinery with four Ca^{2+} binding sites, and a single Ca^{2+} channel. The binding sites range from slow unbinding, high affinity (gate S_1) to fast unbinding, low affinity (gate S_4).*

piecewise constant forcing, it was possible to obtain a geometric series describing release and facilitation as a function of stimulus number. Later we will show that a step-like facilitation curve is produced by a more realistic model in which channel opening and closing is stochastic and the flux through an open channel, and thus Ca, is voltage dependent. In addition, we show that, to leading order, the rise in release and facilitation over a train of pulses is exponential.

2.2. Release evoked by stochastic channel openings. We now describe a more realistic model that takes into account the stochasticity of Ca^{2+} channel openings. We assume that a Ca^{2+} channel has one open and one closed state and replace Ca in (2.2) with $X\,Ca$, where Ca now represents Ca^{2+} concentration in the microdomain surrounding an open channel and X is a random variable equal to 0 if the channel is closed and 1 if the channel is open. As a first step, we focus on the dynamics of one gate. Then the stochastic equation governing the temporal evolution of the concentration of bound gates of this type is

$$\begin{aligned}\frac{dB_j}{dt} &= k_j^+ X\,Ca(V) - (k_j^+ X\,Ca(V) + k_j^-)\,B_j \\ &= f(X, B_j).\end{aligned} \tag{2.4}$$

In [4] this stochastic process was simulated using a Monte Carlo procedure. Time was discretized, and at each time step the state of the Ca^{2+} channel associated with each release site in a population was determined. The evolution of B_j $(j = 1, \ldots, 4)$

at each site then follows from (2.4), with $X = 0, 1$ depending on the state of the channel. The probability of release at the site was then determined as the product $B_1 \cdots B_4$. Finally, mean release was approximated by the sample mean, obtained by dividing the sum of the single-site release probabilities by the number of sites in the population.

The binding of Ca^{2+} to a gate could also be modeled stochastically. The Monte Carlo procedure described above is equivalent to first averaging over all realizations of the binding process, taking it to the deterministic limit, and then averaging over channel states. Below we derive the deterministic limit of the latter averaging process, leading to differential equations for the mean release. In Appendix C we give an alternate derivation for the mean release equations that treats both channels and gates stochastically.

For notational simplicity we drop the subscript denoting the gate number. The probability density function of B is the sum of two components associated with the two possible channel states. We define, for small Δu, the joint probability $p_0(u,t)\,\Delta u = \Pr[B \in (u, u+\Delta u) \text{ and } X = 0]$ for the population of sites associated with closed channels, and $p_1(u,t)\,\Delta u = \Pr[B \in (u, u+\Delta u) \text{ and } X = 1]$ for the population associated with open channels. As channels open and close a given site jumps from one population to the other, and the evolution of the density functions is described by the coupled hyperbolic equations

$$\frac{\partial}{\partial t} p_0(u,t) + \frac{\partial}{\partial u}\left[f(0,u)\, p_0(u,t)\right] = -\alpha(V)\, p_0(u,t) + \beta(V)\, p_1(u,t), \tag{2.5a}$$

$$\frac{\partial}{\partial t} p_1(u,t) + \frac{\partial}{\partial u}\left[f(1,u)\, p_1(u,t)\right] = \alpha(V)\, p_0(u,t) - \beta(V)\, p_1(u,t) \tag{2.5b}$$

for $t > 0$, $u \in (0,1)$. Here α (β) is the voltage-dependent probability per unit time that a closed (open) channel opens (closes) (see Appendix A for details). Equation (2.5a) (or (2.5b)), without the coupling terms, is analogous to the mass conservation equation of a fluid, with f representing fluid velocity and p_0 representing fluid density. It is also the deterministic limit of the Fokker–Planck equation for this process [7].

When uncoupled ($\alpha = \beta = 0$) each population evolves along characteristics determined by

$$\frac{du}{dt} = f(i,u), \tag{2.6a}$$

$$\frac{dp_i}{dt} = -\frac{df}{du}(i,u)\, p_i \tag{2.6b}$$

for $i = 0, 1$. The characteristics for the p_0 population are $u(t) = s\, e^{-k^- t}$, where $s \in [0,1]$ (Fig. 2.2A). The dependent variable p_0 increases exponentially along a characteristic, $p_0(u,t) = p_0(s,0)\, e^{k^- t}$. The p_1 characteristics $u(t) = \bar{u} + (s - \bar{u})\, e^{-(k^+ Ca + k^-)\, t}$ asymptote to $\bar{u} = k^+ Ca\,/(k^+ Ca + k^-)$, the singular point satisfying $f(1,\bar{u}) = 0$ (Fig. 2.2B). Again the dependent variable increases exponentially along a characteristic $p_1(u,t) = p_1(s,0)\, e^{(k^+ Ca + k^-)\, t}$.

When there is no coupling, (2.6a), (2.6b) ensure that mass is conserved in each population provided that the following boundary conditions are applied (see Fig. 2.2):

$$p_0(1,t) = 0,\ p_1(0,t) = 0,\ p_1(1,t) = 0. \tag{2.7}$$

The coupling terms allow mass to flow between populations while conserving the sum of the masses, which we set to 1 through the initial conditions. Thus, p_0 and p_1

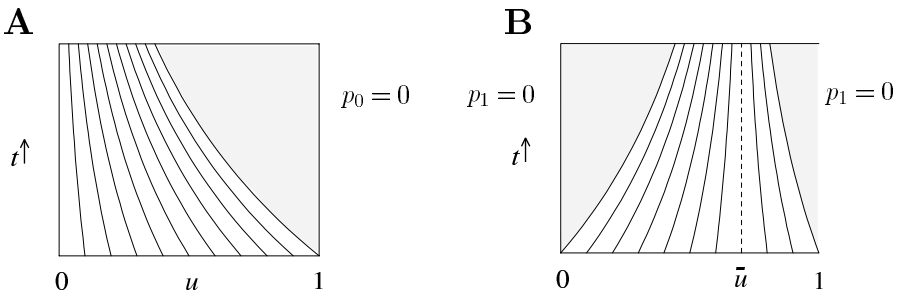

FIG. 2.2. *Characteristics and boundary conditions for the* (A) p_0 *population and the* (B) p_1 *population. The singular value* $\bar{u}$ *satisfies* $f(1, \bar{u}) = 0$.

satisfying (2.5a), (2.5b) with the boundary conditions (2.7) and appropriate initial conditions satisfy the conservation law

$$\int_0^1 p_0(u,t) + p_1(u,t)\, du = 1 \tag{2.8}$$

for each $t \geq 0$.

The transfer rates α and β both depend on voltage, with $\alpha \ll \beta$ at low voltages and $\alpha \gg \beta$ at high voltages. The singular value $\bar{u}$ also inherits a voltage dependence through the factor Ca, although this dependence is typically not important (see Appendix A for expressions and parameter values). If the synapse is hyperpolarized (V negative) for a long period of time, then the p_0 population will contain most of the mass since $\beta \gg \alpha$. Since the characteristics for this population contract toward $u = 0$, the mean concentration of bound gates will be low (Fig. 2.3A). If the synapse is subsequently depolarized (V positive), $\alpha \gg \beta$ and mass will transfer from the p_0 population to the p_1 population, where it will migrate rightward toward $\bar{u}$ with a time constant of $1/(k^+ Ca + k^-)$ (Fig. 2.3B). If the synapse is then hyperpolarized, mass will flow back to the p_0 population and will migrate leftward with a time constant of $1/k^-$ (Fig. 2.3C). If the membrane is again depolarized before the p_0 distribution has returned to its initial state, then the mean of the resulting p_1 distribution will be greater than during the first pulse (Fig. 2.3D). This process of facilitation is particularly evident by the fifth pulse (Fig. 2.3E,F).

2.3. Equations for mean release. Rather than computing the temporal evolution of the probability density functions for the two populations, it is sufficient to follow their expected values when computing the total release from a nerve terminal. Define

$$\sigma^c(t) = \int_0^1 u\, p_0(u,t)\, du, \tag{2.9a}$$

$$\sigma^o(t) = \int_0^1 u\, p_1(u,t)\, du, \tag{2.9b}$$

so that $\sigma = \sigma^c + \sigma^o = \mathrm{E}[B]$, the expected concentration of bound gates of this type. (Because B was defined as normalized concentration, σ can also be thought of as the probability that a gate is bound, while σ^o (σ^c) is the probability that a gate is bound and the associated Ca^{2+} channel is open (closed).) Then, using (2.5b), (2.7), and

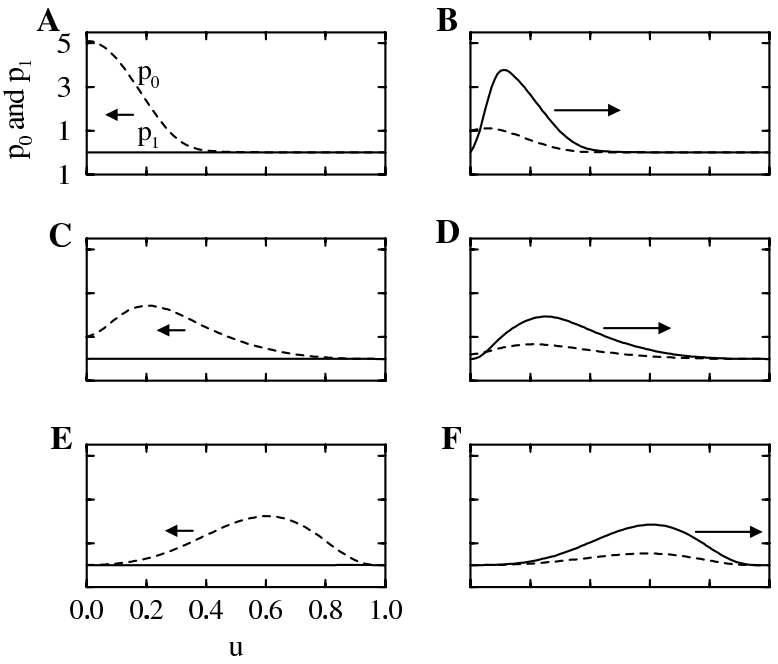

FIG. 2.3. *Solution of* (2.5a), (2.5b) *with boundary conditions* (2.7) *at six different times using the numerical scheme discussed in Appendix B. Simulating a voltage clamp protocol, voltage is periodically pulsed from a hyperpolarized level (*-65 *mV for* 5 *msec) to a depolarized level (*10 *mV for* 1 *msec). Arrows indicate direction of motion of the population means.* (A) *Initial distribution at* $V = -65$ *mV;* (B, D, F) *distributions at the end of the first, second, and fifth depolarizations, respectively;* (C, E) *distributions shortly before the second and fifth depolarizations, respectively. The net rightward displacement of the population means indicates that the gate is facilitating. In this example* $k^+ = 3 \times 10^{-2}$, $k^- = 1 \times 10^{-2}$, *and* $Ca_{ex} = 2$ *mM. All other parameters are as given in the text and in Appendix A.*

integration by parts,

$$
\begin{aligned}
\frac{d\sigma^o}{dt} &= \int_0^1 u \frac{\partial p_1}{\partial t}\, du \\
&= \int_0^1 u \left[-\frac{\partial \left(f(1,u)\, p_1 \right)}{\partial u} + \alpha p_0 - \beta p_1 \right] du \\
&= \int_0^1 f(1,u)\, p_1\, du - f(1,1)\, p_1(1,t) \\
&\quad + \alpha \int_0^1 u\, p_0\, du - \beta \int_0^1 u\, p_1\, du \\
&= \int_0^1 \left[k^+ Ca - (k^+ Ca + k^-)\, u \right] p_1\, du \\
&\quad + \alpha \int_0^1 u\, p_0\, du - \beta \int_0^1 u\, p_1\, du.
\end{aligned} \tag{2.10}
$$

We now define $m \equiv \Pr[X = 1] = \int_0^1 p_1\, du$, so that

$$
\frac{d\sigma^o}{dt} = k^+ Ca\, m - (k^+ Ca + k^-)\, \sigma^o + \alpha\, \sigma^c - \beta\, \sigma^o. \tag{2.11a}
$$

Similarly,

$$\frac{d\sigma^c}{dt} = -k^- \sigma^c - \alpha \sigma^c + \beta \sigma^o, \tag{2.11b}$$

and thus

$$\frac{d\sigma}{dt} = -k^- \sigma - k^+ Ca\, \sigma^o + k^+ Ca\, m. \tag{2.11c}$$

The rate of change of m is determined by the Ca^{2+} channel kinetics

$$\frac{dm}{dt} = \alpha (1 - m) - \beta m. \tag{2.12}$$

Thus, the equations for the expected values of p_0 and p_1 are linear with time-dependent coefficients α, β, and Ca and with time-dependent forcing by Ca and m.

If release sites contained a single gate, (2.11a) and (2.11b) with the auxiliary equation (2.12) would completely describe the mean release. Our model, however, postulates four gates per release site. In this case, equations like (2.11a) and (2.11b) describe the expected concentration of bound gates of any one of the four types, denoted $\sigma_1, \ldots, \sigma_4$. Since the gates are correlated through m and Ca, $\mathrm{E}[R] = \mathrm{E}[B_1 B_2 B_3 B_4] \neq \sigma_1 \sigma_2 \sigma_3 \sigma_4$. Intuitively, since all four gates at a release site respond to Ca^{2+} influx through the same Ca^{2+} channel, if a gate is bound then it is more likely that the channel is open than if the gate is unbound. Hence, it is more likely that one of the other gates is bound. In the Monte Carlo simulations performed in [4], this result is equivalent to the observation that to compute the sample mean of release one must take the sample mean of the product of the B_j's at each site in the ensemble rather than taking the product of the sample means of the B_j's.

Thus, to compute mean release we must consider the joint density functions $p_i(\vec{u}, t) = p_i(u_1, u_2, u_3, u_4, t)$, $i = 0, 1$. We define the vector function $\vec{f}(i, \vec{u}) = (f_1(i, u_1), f_2(i, u_2), f_3(i, u_3), f_4(i, u_4))^T$, $i = 0, 1$, with each component defined as in (2.4). We then extend (2.5a) and (2.5b),

$$\frac{\partial}{\partial t} p_0(\vec{u}, t) + \nabla_u \cdot \left[\vec{f}(0, \vec{u})\, p_0(\vec{u}, t) \right] = -\alpha\, p_0(\vec{u}, t) + \beta\, p_1(\vec{u}, t), \tag{2.13a}$$

$$\frac{\partial}{\partial t} p_1(\vec{u}, t) + \nabla_u \cdot \left[\vec{f}(1, \vec{u})\, p_1(\vec{u}, t) \right] = \alpha\, p_0(\vec{u}, t) - \beta\, p_1(\vec{u}, t), \tag{2.13b}$$

where $\nabla_u = (\frac{\partial}{\partial u_1}, \frac{\partial}{\partial u_2}, \frac{\partial}{\partial u_3}, \frac{\partial}{\partial u_4})^T$. The boundary conditions generalize naturally so that $p_0(\vec{u}, t) = 0$ if any component $u_j = 1$, and $p_1(\vec{u}, t) = 0$ if any $u_j = 0$ or 1.

Define

$$\sigma^c_{1234}(t) = \int\int\int\int_0^1 u_1\, u_2\, u_3\, u_4\, p_0(\vec{u}, t)\, d\vec{u}, \tag{2.14a}$$

$$\sigma^o_{1234}(t) = \int\int\int\int_0^1 u_1\, u_2\, u_3\, u_4\, p_1(\vec{u}, t)\, d\vec{u}, \tag{2.14b}$$

and then $\sigma_{1234} = \sigma^c_{1234} + \sigma^o_{1234} = E[R]$. The marginal expectations σ_{jkl}, σ_{jk}, and σ_j are defined analogously. As before, we construct differential equations for the expectations by differentiating σ^c_{1234} and σ^o_{1234}, substituting the partial differential

equations (2.13a), (2.13b), and using integration by parts. This yields

$$\frac{d\sigma^c_{1234}}{dt} = -\sum_{j=1}^{4} k_j^- \sigma^c_{1234} - \alpha\,\sigma^c_{1234} + \beta\,\sigma^o_{1234}, \tag{2.15a}$$

$$\frac{d\sigma^o_{1234}}{dt} = -\sum_{j=1}^{4} \left(k_j^+\,Ca + k_j^-\right)\,\sigma^o_{1234} + \alpha\,\sigma^c_{1234} - \beta\,\sigma^o_{1234} + \left(k_1^+\,\sigma^o_{234} + k_2^+\,\sigma^o_{341} + k_3^+\,\sigma^o_{412} + k_4^+\,\sigma^o_{123}\right)\,Ca. \tag{2.15b}$$

Differential equations for the marginal expectations appearing in (2.15b) are obtained following a similar procedure. For each triplet $qrs = 234, 341, 412,$ and 123,

$$\frac{d\sigma^c_{qrs}}{dt} = -\sum_{j=q,r,s} k_j^- \sigma^c_{qrs} - \alpha\,\sigma^c_{qrs} + \beta\,\sigma^o_{qrs}, \tag{2.15c}$$

$$\frac{d\sigma^o_{qrs}}{dt} = -\sum_{j=q,r,s} \left(k_j^+\,Ca + k_j^-\right)\,\sigma^o_{qrs} + \alpha\,\sigma^c_{qrs} - \beta\,\sigma^o_{qrs} + \left(k_q^+\,\sigma^o_{rs} + k_r^+\,\sigma^o_{sq} + k_s^+\,\sigma^o_{qr}\right)\,Ca. \tag{2.15d}$$

Similarly, for each doublet $qr = 12, 13, 14, 23, 24,$ and 34 (the order of indices is unimportant, e.g., $\sigma_{12} = \sigma_{21}$),

$$\frac{d\sigma^c_{qr}}{dt} = -\sum_{j=q,r} k_j^- \sigma^c_{qr} - \alpha\,\sigma^c_{qr} + \beta\,\sigma^o_{qr}, \tag{2.15e}$$

$$\frac{d\sigma^o_{qr}}{dt} = -\sum_{j=q,r} \left(k_j^+\,Ca + k_j^-\right)\,\sigma^o_{qr} + \alpha\,\sigma^c_{qr} - \beta\,\sigma^o_{qr} + \left(k_q^+\,\sigma^o_{r} + k_r^+\,\sigma^o_{q}\right)\,Ca. \tag{2.15f}$$

Finally, differential equations for σ^c_q, σ^o_q ($q = 1, 2, 3, 4$) and the calcium channel open probability m have been derived earlier and are given by (2.11b), (2.11a), and (2.12), respectively. Expected release, then, depends upon the mean concentrations of all gate configurations and is completely described by $2\,(1+4+6+4) = 30$ differential equations along with an auxiliary equation for m. This is easily generalized, so that for a model with M gates per release site and N distinct Ca^{2+} channel states the number of equations describing mean release is $N\,(2^M - 1)$, plus auxiliary equations for membrane potential and the gating of Ca^{2+} channels.

Release and facilitation, the ratio of release evoked by the nth stimulus to that evoked by the first during a 30 Hz train of presynaptic stimuli is illustrated in Fig. 2.4. Each stimulus consists of a 2 msec voltage depolarization to 10 mV from a resting level of −65 mV (Fig. 2.4A). Solving the equations numerically for expected release, we see that evoked release grows monotonically with each stimulus. This facilitation is due primarily to the accumulation of bound calcium to the two slowest gates (Fig. 2.4C). Gate S_3 loses Ca^{2+} too quickly to contribute much to facilitation during the 30 Hz stimulus train (Fig. 2.4B), although at higher frequencies its contribution can be considerable. Gate S_4 is too fast to contribute to facilitation at any stimulus frequency,

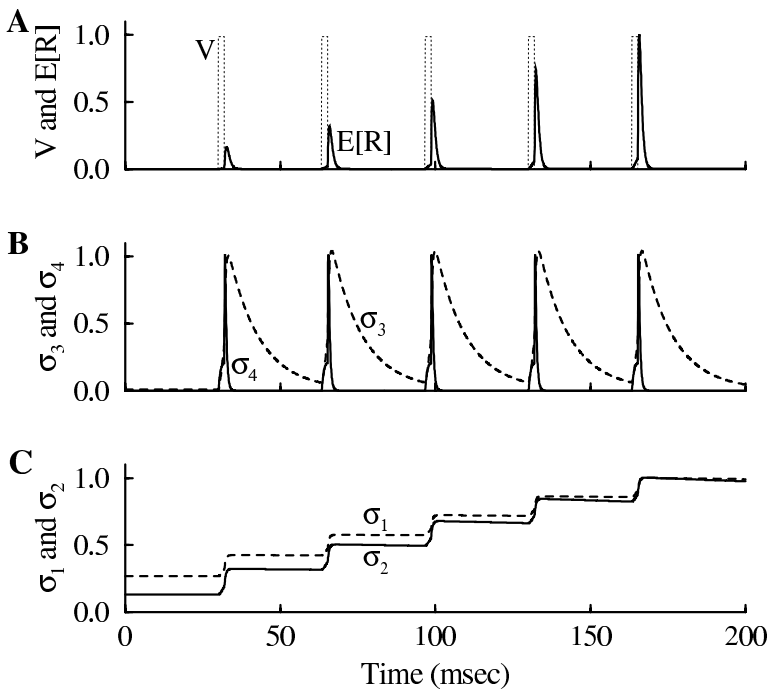

FIG. 2.4. *Numerical solution of the* 30 *equations describing transmitter release,* (2.11a), (2.11b), (2.15a)–(2.15f), *plus the auxiliary equation* (2.12). *A series of* 2*-msec depolarizing pulses to* 10 mV *is applied from a holding potential of* -65 mV. *With this* 30 *Hz stimulation* Ca^{2+} *unbinds from gate* S_3 *too quickly for the gate to contribute to facilitation* (B). *The low unbinding rates of gates* S_1 *and* S_2 *allow bound* Ca^{2+} *to accumulate* (C), *yielding a facilitated release* (A). *Each record is normalized by its maximum value during the fifth pulse. The nonnormalized values of* σ_1 *and* σ_2 *are much greater than* σ_3 *and* σ_4 *due to their smaller dissociation constants. The standard parameter set is used, with* $Ca_{ex} = 1$ mM. *The differential equations are solved here and in Figs.* 3.1, 4.1, 5.1 *using a variable-step Adams method with tolerance* 10^{-9}.

its primary role being to terminate release soon after the end of the presynaptic stimulus. Notice that most of the release occurs after the depolarizing step (during the so-called tail), when the product mCa is greatest. The time course of the fall of release reflects the time course of Ca^{2+} channel closure.

3. Steps in the frequency dependence of facilitation. We saw in Fig. 2.4 that the degree of facilitation achieved during a short train of stimuli depends crucially on both the frequency at which the stimuli are applied and the binding and unbinding rates of the three slow gates. This is true also of the asymptotic facilitation, or facilitation achieved over a long stimulus train. With the deterministic model we showed [4] that the asymptotic facilitation of each slow gate increases in a sigmoidal fashion with the stimulus frequency when viewed on a log-linear scale. That is, at low frequencies there is little or no facilitation, while at very high frequencies the slow gate saturates and facilitation approaches some maximum value. At frequencies between these two extremes the increase in single-gate facilitation with stimulus frequency is approximately linear. The half-maximal frequency for each sigmoid depends upon the unbinding time constant of the gate, with slower gates having lower half-maximal frequencies. Since the release is the product of the concentrations of bound gates, the facilitation of release was easily computed as the product of three

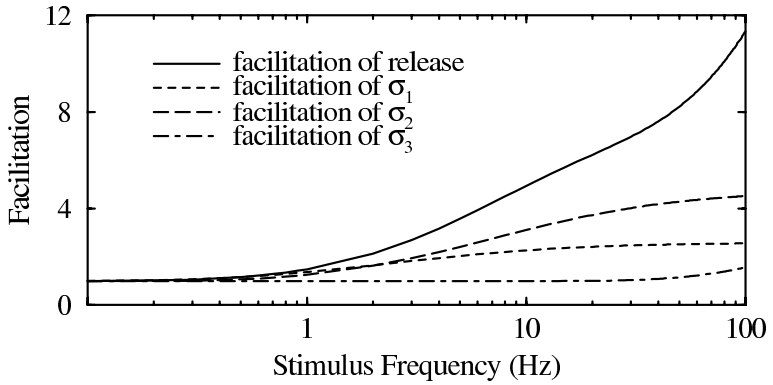

FIG. 3.1. *Step-like dependence of facilitation on stimulus frequency (solid curve) and the contribution from each of the three slow gates. The method used to construct the curves is described in the text. The standard parameter set is used, with* $Ca_{ex} = 10$ *mM.*

sigmoids (on a log-linear scale), yielding a step-like asymptotic facilitation curve consistent with data from the squid giant synapse stimulated by long trains of action potentials [21].

Because the stimulus train evoking release with the deterministic model consisted of square pulses of Ca^{2+} rather than action potentials, the deterministic facilitation curve may be qualitatively different from that computed with the more realistic stochastic model. In principle we could have constructed the stochastic facilitation curve using the Monte Carlo algorithm in [4], but the required computer time was prohibitive since thousands of sites are required for the sample mean to accurately approximate the true mean. With the present method, construction of the stochastic facilitation curve is now feasible. This requires the numerical solution of the 30 differential equations describing mean release coupled to a four-variable Hodgkin–Huxley-like system describing a nerve impulse (see Appendix A). Short, impulse-inducing current pulses are applied to the system at frequencies ranging from 0.1 to 100 Hz. The number of current pulses applied at each frequency is large enough to allow facilitation to reach steady state. Facilitation of each of the marginal expectations σ_1, σ_2, and σ_3 exhibits a sigmoidal frequency dependence (Fig. 3.1), and the product of the three single-gate facilitation curves has a step-like appearance (not shown), as does the true facilitation curve (solid curve in Fig. 3.1). (We show later that the product of the three single-gate facilitation functions is approximately equal to the true facilitation function.) This is the first model of transmitter release to reproduce this behavior.

4. Multiple scale analysis.

4.1. Single-gate facilitation. In this section we use a mutiple scale perturbation analysis to better understand the process of facilitation. We show that the facilitation provided by each of the slow gates rises exponentially in time and depends only on the average domain Ca^{2+} concentration, rather than the detailed distribution of Ca^{2+} domains. This allows us to construct a leading-order formula for facilitation. In section 4.2 we show that facilitation of release is, to leading order, the product of the single-gate facilitation functions. This has all the qualitative features of the facilitation curve shown in section 3, including its step-like frequency dependence.

In the multiple scale analysis we take advantage of the fact that for gates S_1, S_2, and S_3 the binding (k^+) and unbinding (k^-) parameters are small compared with other parameters. The intuition is that for the slow gates the binding time course consists of rapid oscillations (on the channel time scale) superimposed on a slowly facilitating base (Fig. 2.4C). We are interested in the behavior of the system during a long train of periodically applied voltage-clamp depolarizations or impulse-generating current pulses, and we assume that the system is at equilibrium prior to the onset of these stimuli.

First the system is put into a nondimensional form. As a representative time scale we take the time constant for the Ca^{2+} activation variable m, $\tau_m(V) = 1/(\alpha(V) + \beta(V))$, evaluated at $V = -65$ mV. For notational simplicity we write all dimensional variables with a tilde and define the dimensionless time as $t = \tilde{t}/\tau_m$. With this scaling (2.11b) becomes

$$\frac{d\sigma^c}{dt} = -\epsilon\sigma^c - \alpha\,\sigma^c + \beta\,\sigma^o, \tag{4.1a}$$

where $\alpha = \tilde{\alpha}\,\tau_m$, $\beta = \tilde{\beta}\,\tau_m$, and $\epsilon = k^-\,\tau_m$. Because the unbinding rate from the gates is small, $\epsilon \ll 1$. Likewise, (2.11a) becomes

$$\frac{d\sigma^o}{dt} = \epsilon\bar{c} - \epsilon(c+1)\sigma^o + \alpha\,\sigma^c - \beta\,\sigma^o, \tag{4.1b}$$

where $c = \frac{Ca}{K_D}$, $K_D = \frac{k^-}{k^+}$ is the dissociation constant of the gate, and $\bar{c} = cm$ is the population-averaged domain Ca^{2+} concentration. That is, $\bar{c}$ is the dimensionless domain Ca^{2+} concentration at an open Ca^{2+} channel multiplied by the fraction of open channels. The rate of change of the concentration of bound gates, $\sigma = \sigma^c + \sigma^o$, is

$$\frac{d\sigma}{dt} = -\epsilon\sigma - \epsilon c\,\sigma^o + \epsilon\bar{c}. \tag{4.1c}$$

The nondimensional forms of (2.12) and (2.15a)–(2.15f) are analogous.

We now introduce the slow time $\tau = \epsilon\,t = k^-\,\tilde{t}$, which will be the time scale of facilitation, and the multiple scale expansion $\sigma(t,\tau) = \sigma_0(t,\tau) + \epsilon\sigma_1(t,\tau) + \mathcal{O}(\epsilon^2)$, with similar expansions for σ^c and σ^o. Introducing these expansions into (4.1a)–(4.1c) and collecting terms with like powers of ϵ, we obtain the $\mathcal{O}(1)$ system

$$\frac{\partial\sigma_0^c}{\partial t} = -\alpha\sigma_0^c + \beta\sigma_0^o, \tag{4.2a}$$

$$\frac{\partial\sigma_0^o}{\partial t} = \alpha\sigma_0^c - \beta\sigma_0^o, \tag{4.2b}$$

$$\frac{\partial\sigma_0}{\partial t} = 0 \tag{4.2c}$$

(subscripts correspond to powers of ϵ and superscripts to the state of the channel). Thus, on the fast time scale there is a transfer of mass between the open channel population and the closed channel population while the concentration of bound gates, σ_0, is conserved. That is, σ_0 changes only on the slow time scale τ: $\sigma_0 = \sigma_0(\tau)$.

In addition to this conservation property, the $\mathcal{O}(1)$ system has the property that the state of the Ca^{2+} channel (open or closed) and the state of the gate (bound or unbound) are statistically independent:

$$\sigma_0^o = m\,\sigma_0. \tag{4.3}$$

That is, the probability that the channel is open and the gate is bound is simply the product of the probability that the channel is open and the probability that the gate is bound. To show this we consider

$$\begin{aligned}\frac{\partial}{\partial t}(\sigma_0^o - m\sigma_0) &= \frac{\partial \sigma_0^o}{\partial t} - \frac{dm}{dt}\,\sigma_0 - m\,\frac{\partial \sigma_0}{\partial t} \\ &= \alpha\sigma_0^c - \beta\sigma_0^o - [\alpha - (\alpha+\beta)m]\,\sigma_0 \\ &= -(\alpha+\beta)(\sigma_0^o - m\sigma_0),\end{aligned} \tag{4.4}$$

which implies $\sigma_0^o - m\sigma_0$ decays exponentially to zero. Since we assume that the initial state of the system is at equilibrium prior to the onset of stimulation, $\sigma_0^o = m\sigma_0$ at time 0 and (4.4) implies that this equality holds for all time.

The $\mathcal{O}(\epsilon)$ equation for the expected concentration of bound gates is

$$\begin{aligned}\frac{\partial \sigma_1}{\partial t} &= -\frac{\partial \sigma_0}{\partial \tau} - \sigma_0 - c\sigma_0^o + \bar{c} \\ &= -\frac{\partial \sigma_0}{\partial \tau} - \sigma_0 - \bar{c}\sigma_0 + \bar{c},\end{aligned} \tag{4.5}$$

where we have used the independence property (4.3). This equation has a periodic solution on a fast time scale provided that the following Fredholm condition is satisfied:

$$\frac{1}{T}\int_0^T \left[-\frac{\partial \sigma_0}{\partial \tau} - (1+\bar{c})\,\sigma_0 + \bar{c}\right]\,dt = 0, \tag{4.6}$$

where T is the stimulus period. This can be rewritten as

$$\frac{\partial \sigma_0}{\partial \tau} = -(1+\langle \bar{c} \rangle)\,\sigma_0 + \langle \bar{c} \rangle, \tag{4.7}$$

where $\langle \bar{c} \rangle \equiv \frac{1}{T}\int_0^T \bar{c}\,dt$, the time- and population-averaged domain Ca, and we have used the fact that σ_0 is constant over a period. If the stimulus is periodic, $\langle \bar{c} \rangle$ is constant, and (4.7) has a simple exponential solution

$$\sigma_0(\tau) = \frac{\langle \bar{c} \rangle}{1+\langle \bar{c} \rangle} + \left(\sigma_0(0) - \frac{\langle \bar{c} \rangle}{1+\langle \bar{c} \rangle}\right)\,e^{-(1+\langle \bar{c} \rangle)\tau}, \tag{4.8}$$

where $\sigma_0(0)$ is the initial value of σ_0. The exponential rise in σ_0 during a train of depolarizations is demonstrated in Fig. 4.1A for two different concentrations of calcium. The solid curves are generated by solving (4.1b) and (4.1c) and show the evolution of the full solution (σ) for each Ca^{2+} concentration. The dashed curves are generated from (4.8) and show the evolution of σ_0, clearly capturing the slow growth of the full solution.

Equation (4.8) describes the slow growth of the average value of σ due to the periodically applied depolarizations or impulses and thus can be used to provide an $\mathcal{O}(1)$ measure of the time-dependent facilitation of the gate. Thus, facilitation (F) is approximately $\sigma_0(\tau)/\sigma_0(\epsilon T)$, the ratio of σ_0 at τ to its value at the end of the first period. This tells us that single-gate facilitation depends only on $\langle \bar{c} \rangle$, and not the detailed distribution of Ca^{2+} domains. It also allows us to predict that the rate of convergence of facilitation to its asymptotic value increases with the average Ca^{2+} concentration, generalizing the same result found with the deterministic model of

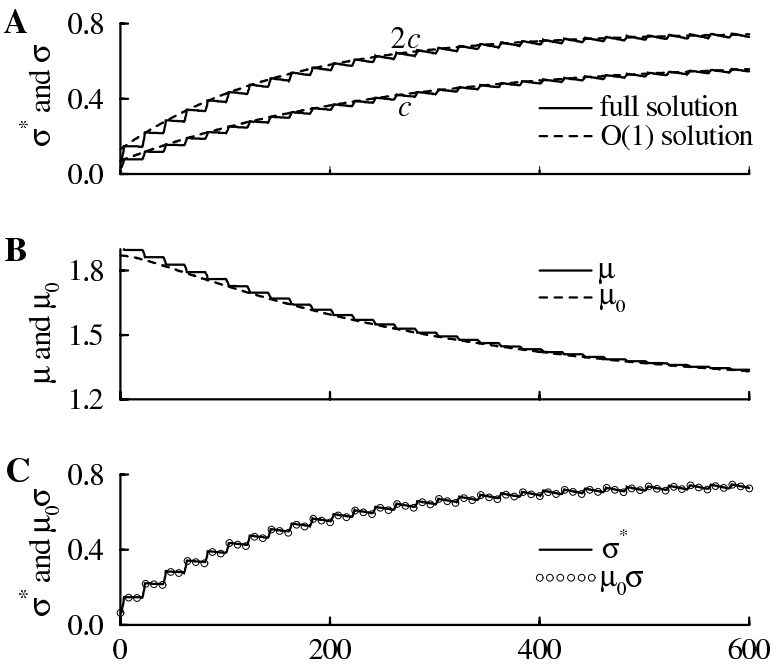

FIG. 4.1. (A) *Numerical solution of* (4.1b), (4.1c) *(solid) and evaluation of* (4.8) *(dashed) for two values of dimensionless calcium* (σ *and* σ^**). See the text for a more detailed description. The stimulus train consists of* 30 *depolarizations from* -65 *to* 10 mV *each for a duration of* 2 *msec, with* 18 *msec between depolarizations. Prior to the onset of stimulation the system was allowed to reach equilibrium at* $V = -65$ mV*. For the bottom curves* $Ca_{ex} = 1$ mM*, for the top* $Ca_{ex} = 2$ mM*.* (B) *t-dependent ratio* μ *(solid) and* τ*-dependent normalization factor* μ_0 *(dashed).* (C) *Demonstration of time course invariance. When* σ *is scaled up by the* $\mathcal{O}(1)$ *normalization factor* μ_0 *(circles) it has a time course almost identical to that of* σ^* *(solid).*

section 2.1 [4]. Finally, σ_0 has the asymptotic value $\sigma_0(\infty) = \langle\bar{c}\rangle/(1 + \langle\bar{c}\rangle)$ and has initial value $\sigma_0(0) = \bar{c}(0)/(1+\bar{c}(0))$ (assuming the system starts at equilibrium), where $\bar{c}(0)$ is $\bar{c}$ at the initial voltage. Hence,

$$F_0(\infty) = \frac{\sigma_0(\infty)}{\sigma_0(\epsilon T)} = \frac{\langle\bar{c}\rangle}{1+\langle\bar{c}\rangle}\left[\frac{\langle\bar{c}\rangle}{1+\langle\bar{c}\rangle} + \left(\frac{\bar{c}(0)}{1+\bar{c}(0)} - \frac{\langle\bar{c}\rangle}{1+\langle\bar{c}\rangle}\right) e^{-(1+\langle\bar{c}\rangle)\,\epsilon T}\right]^{-1}. \tag{4.9}$$

In the limit $\epsilon \to 0$,

$$F_0(\infty) \to \frac{\langle\bar{c}\rangle\,(1+\bar{c}(0))}{(1+\langle\bar{c}\rangle)\,\bar{c}(0)} = \frac{\sigma_0(\infty)}{\sigma_0(0)}. \tag{4.10}$$

Typically $\langle\bar{c}\rangle > \bar{c}(0)$, so $\sigma_0(\infty)$ is more saturated than $\sigma_0(0)$. Hence, increasing Ca_{ex} will increase $\sigma_0(0)$ more than $\sigma_0(\infty)$ and facilitation will decline, generalizing another result found with the deterministic model [4]. This decline in facilitation can also be observed by plotting (4.9). As $\langle\bar{c}\rangle$ is increased, $F_0(\infty)$ decreases monotonically (not shown).

At moderate-to-high frequencies the relationship between stimulus frequency and $\langle\bar{c}\rangle$ is nearly linear since a change in frequency corresponds to a change in the time

between stimuli, during which $\bar{c}$ is nearly zero (the interstimulus contribution becomes substantial at low frequencies and cannot be neglected; see (4.18)). Therefore, (4.10) shows that for a very slow gate ($\epsilon \approx 0$) there is a hyperbolic relationship between stimulus frequency and single-gate asymptotic facilitation. On a log-linear scale this relation is sigmoidal, consistent with our previous numerical calculation of single-gate facilitation (Fig. 3.1).

4.2. Facilitation of release. How do these single-gate facilitation results extend to facilitation of the full system, that is, to facilitation of release? We show below that gate S_4 contributes little to facilitation of release (i.e., the gate has no memory), so facilitation is due almost entirely to facilitation of σ_{123}. Although $\sigma_{123} \neq \sigma_1 \sigma_2 \sigma_3$, we show that $\sigma_{123,0} = \sigma_{1,0} \sigma_{2,0} \sigma_{3,0}$ (the second index denotes the order of the term in the perturbation expansion). This is consistent with the intuition that the gates are correlated only because of the correlation between the Ca^{2+} channel and each gate. In the leading-order system the gates and channel are statistically independent ($\sigma^o_{j,0} = m\,\sigma_{j,0}$), so the correlation among the gates is removed. The product of the leading-order single-gate facilitation functions thus provides a leading-order approximation to the facilitation of release.

To show that gate S_4 does not affect facilitation, consider σ_{j4} where $j = 1, 2$, or 3. Since S_4 is fast (i.e., k_4^- is large), σ_{j4} can be assumed to be in quasi equilibrium with the domain Ca^{2+} concentration. Let σ^*_{j4} denote the peak value of σ_{j4} during the nth pulse, and denote its peak value during the first pulse simply by σ_{j4}. Then the facilitation of this joint expectation, F_{j4}, is (in terms of dimensional parameters)

$$F_{j4} = \frac{k_4^+ \sigma_j^{o*} + k_j^+ \sigma_4^{o*}}{k_4^+ \sigma_j^o + k_j^+ \sigma_4^o}. \tag{4.11}$$

Since the dissociation constant (k^-/k^+) is much greater for the fast gate than any of the slow gates, $\sigma_j^o \gg \sigma_4^o$; hence,

$$F_{j4} \approx \frac{\sigma_j^{o*}}{\sigma_j^o}. \tag{4.12}$$

From the analysis in section 4.1, $\sigma_j^o \approx m\,\sigma_j$; thus

$$F_{j4} \approx F_j, \tag{4.13}$$

where F_j denotes facilitation of the slow gate S_j. This result extends to joint expectations involving S_4 with any combination of slow gates.

Rather than showing directly that $\sigma_{123,0} = \sigma_{1,0} \sigma_{2,0} \sigma_{3,0}$, we show that $\sigma_{qr,0} = \sigma_{q,0} \sigma_{r,0}$ for any doublet $qr = 12$, 13, and 23. We do this by showing that $\sigma_{qr,0}$ and $\sigma_{q,0} \sigma_{r,0}$ satisfy the same differential equations. This result then easily generalizes to joint expectations involving any combination of slow gates. Using the same scaling as before, but with $\epsilon = k_q^- \tau_m$ and Ca scaled by $K_D = k_q^-/k_q^+$, we write (4.1c) and the combined equations (2.15e), (2.15f) in the following nondimensional form:

$$\frac{d\sigma_q}{dt} = -\epsilon\,\sigma_q - \epsilon\,c\,\sigma_q^o + \epsilon\,\bar{c}, \tag{4.14a}$$

$$\frac{d\sigma_r}{dt} = -\epsilon\,k_{qr}^-\,\sigma_r - \epsilon\,k_{qr}^+\,c\,\sigma_r^o + \epsilon\,k_{qr}^+\,\bar{c}, \tag{4.14b}$$

$$\frac{d\sigma_{qr}}{dt} = -\epsilon\,(1 + k_{qr}^-)\,\sigma_{qr} - \epsilon\,c\,(1 + k_{qr}^+)\,\sigma_{qr}^o + \epsilon\,c\,(\sigma_r^o + k_{qr}^+\,\sigma_q^o), \tag{4.14c}$$

where $k_{qr}^- = k_r^-/k_q^-$ and $k_{qr}^+ = k_r^+/k_q^+$. Introducing multiple scale expansions for σ_q, σ_r, and σ_{qr}, it is clear from inspection that $\sigma_{q,0}$, $\sigma_{r,0}$, and $\sigma_{qr,0}$ are all constant over a period (i.e., they vary only on the slow time scale τ). Using the Fredholm condition for periodic solutions of the $\mathcal{O}(\epsilon)$ system, we obtain the slow evolution equations

$$\frac{\partial \sigma_{q,0}}{\partial \tau} = -(1 + \langle \bar{c} \rangle)\, \sigma_{q,0} + \langle \bar{c} \rangle, \tag{4.15a}$$

$$\frac{\partial \sigma_{r,0}}{\partial \tau} = -(k_{qr}^- + k_{qr}^+ \langle \bar{c} \rangle)\, \sigma_{r,0} + k_{qr}^+ \langle \bar{c} \rangle, \tag{4.15b}$$

$$\frac{\partial \sigma_{qr,0}}{\partial \tau} = -(1 + \langle \bar{c} \rangle + k_{qr}^- + k_{qr}^+ \langle \bar{c} \rangle)\, \sigma_{qr,0} + (\sigma_{r,0} + k_{qr}^+ \sigma_{q,0})\, \langle \bar{c} \rangle. \tag{4.15c}$$

Now,

$$\begin{aligned} \frac{\partial}{\partial \tau}\, [\sigma_{q,0}\, \sigma_{r,0}] &= \sigma_{q,0}\, \frac{\partial \sigma_{r,0}}{\partial \tau} + \sigma_{r,0}\, \frac{\partial \sigma_{q,0}}{\partial \tau} \\ &= -(1 + \langle \bar{c} \rangle + k_{qr}^- + k_{qr}^+ \langle \bar{c} \rangle)\, \sigma_{q,0}\, \sigma_{r,0} \\ &\quad + (\sigma_{r,0} + k_{qr}^+ \sigma_{q,0})\, \langle \bar{c} \rangle, \end{aligned} \tag{4.16}$$

which is identical to the $\sigma_{qr,0}$ equation. Therefore, since we assume that the system starts from equilibrium, $\sigma_{qr,0} = \sigma_{q,0}\, \sigma_{r,0}$ for all time.

Having established to leading order the statistical independence of the slow gates, we now compute the leading-order asymptotic facilitation of release ($F_{rel,0}$) by multiplying together the slow-gate leading-order facilitation functions (4.9):

$$\begin{aligned} F_{rel,0}(\infty) &= F_{1,0}(\infty)\, F_{2,0}(\infty)\, F_{3,0}(\infty) \\ &= \prod_{j=1}^{3} \frac{\langle \bar{c} \rangle}{\kappa_{1j} + \langle \bar{c} \rangle} \left[\frac{\langle \bar{c} \rangle}{\kappa_{1j} + \langle \bar{c} \rangle} + \left(\frac{\bar{c}(0)}{\kappa_{1j} + \bar{c}(0)} - \frac{\langle \bar{c} \rangle}{\kappa_{1j} + \langle \bar{c} \rangle} \right) \mathrm{e}^{-(k_{1j}^- + k_{1j}^+ \langle \bar{c} \rangle)\, \epsilon\, T} \right]^{-1}, \end{aligned} \tag{4.17}$$

where $\epsilon = k_1^-\, \tau_m$, $\kappa_{1j} = k_{1j}^-/k_{1j}^+$, and $\kappa_{11} = k_{11}^- = k_{11}^+ = 1$.

To compute the frequency dependence of facilitation we first establish an accurate relation between $\langle \bar{c} \rangle$ and the stimulus frequency ω. As in Fig. 3.1, we use action potentials to evoke release. Assuming that $Ca_{ex} = 10$ mM, average domain Ca^{2+} summed over an action potential (duration 3 msec) is determined numerically to be approximately 63 μM (this must be divided by $K_D = k_1^-/k_1^+$ to get a dimensionless value). For the remainder of the stimulus period (period $= T\, \tau_m$ with units of msec) the membrane potential is approximately constant at -65 mV, and average domain Ca^{2+} at this voltage is 0.038 μM. Therefore,

$$\begin{aligned} \langle \bar{c} \rangle &\approx [63 + 0.038\, (T\, \tau_m - 3)] \,/\, (T\, \tau_m\, K_D) \\ &= [63\, \omega + 0.038\, (1000 - 3\omega)\,] \,/\, 1000 K_D, \end{aligned} \tag{4.18}$$

where $\omega = 1000/(T\, \tau_m)$.

The functions $F_{rel,0}(\infty)$, $F_{1,0}(\infty)$, $F_{2,0}(\infty)$, and $F_{3,0}(\infty)$ are combined with (4.18) to produce the leading-order facilitation curves (solid) in Fig. 4.2. These agree well with the actual facilitation curves (dashed) taken directly from Fig. 3.1, which were constructed by numerical simulation with the full model. Equation (4.17) accurately represents the qualitative features of facilitation, including its step-like appearance. Thus, it can be used to qualitatively analyze the effects of changes in parameter values.

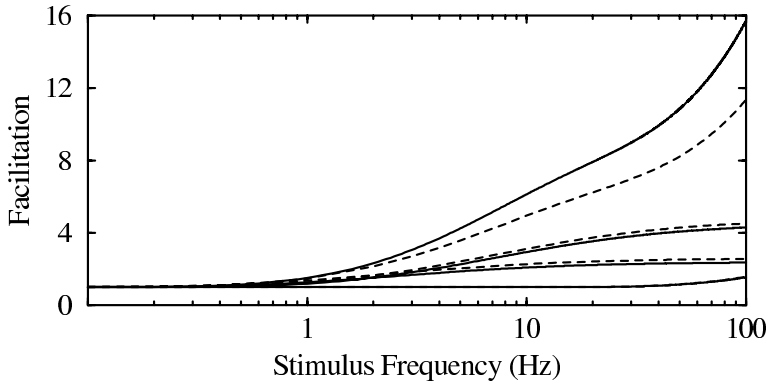

FIG. 4.2. *Facilitation curves taken from Fig.* 3.1 *(dashed) and computed from* (4.17) *with* (4.18) *(solid). The single-gate facilitation curves are sigmoidal, while the total facilitation of release is step-like. As in Fig.* 3.1, *release was evoked by trains of action potentials and* $Ca_{ex} = 10$ *mM.*

Because the difference between $F_{j,0}(\infty)$ and the actual single-gate facilitation is small, the discrepancy between $F_{rel,0}(\infty)$ and the true facilitation of release must lie elsewhere. Most of the error is due to the approximation of σ_{123} with $\sigma_{123,0}$. This approximation is good only to leading order, and the coefficient of the error term may be large. Additional error is introduced because σ_{1234} is used to compute facilitation of release with the full model, while only the three slow gates are used for facilitation in (4.17), but this error is quantitatively small.

4.3. Time course of release unchanged by changes in Ca_{ex}. One property of synaptic release exhibited in our earlier Monte Carlo simulations [4] is the so-called time course invariance property. In experiments with a mammalian neuromuscular junction [6], release was evoked with external Ca^{2+} concentrations of 0.5 mM and 1.0 mM, and the two release time courses were normalized to have the same peak values. When the normalized records were superimposed, they were indistinguishable. Further simulations with the present form of the model (not shown) suggest that this invariance property is valid over the entire range of physiological external Ca^{2+} concentrations (0.5–10 mM). In addition, the model shows that this property holds during each pulse in a train of impulses, in spite of the fact that the release facilitates and the degree of facilitation is dependent upon Ca_{ex}. In this section we demonstrate that the invariance is a fundamental feature of the model by showing that the time-dependent normalization factor is constant with respect to the fast time t, varying only with the slow time τ (to leading order). In other words, release scales uniformly over the duration of a single impulse.

We first investigate the effects on a single slow gate of raising Ca_{ex}. We assume in the model that domain Ca^{2+} concentration is proportional to Ca_{ex}, but this is not necessary to prove invariance. We only require that c increase with Ca_{ex}. Denoting by σ^* the corresponding value of σ, we define the normalization factor as the ratio

$$\mu(t,\tau) = \frac{\sigma^*(t,\tau)}{\sigma(t,\tau)}. \tag{4.19}$$

We now show that $\mu = \mu(\tau)$ for a slow gate, to leading order. Using the expansion $\mu(t,\tau) = \mu_0(t,\tau) + \mathcal{O}(\epsilon)$ in (4.19) along with expansions for σ^* and σ, we obtain for

the $\mathcal{O}(1)$ system,

$$\mu_0 = \frac{\sigma_0^*}{\sigma_0}. \tag{4.20}$$

From (4.8) we know that σ_0 and σ_0^* depend only on τ, so the same is true for μ_0. Thus, $\mu(t,\tau) = \mu_0(\tau) + \mathcal{O}(\epsilon)$, establishing the invariance property to first order.

The approximation μ_0 to μ and the invariance property are illustrated numerically in Fig. 4.1. As discussed earlier, Fig. 4.1A shows the evolution of σ and σ_0 for a slow gate (S_1) over a train of voltage-clamp depolarizations. The upper set of curves corresponds to a concentration of Ca^{2+} twice that of the lower curves. In Fig. 4.1B the ratio μ defined in (4.19) (solid) and the ratio μ_0 expressed in (4.20) (dashed) are shown. The initial normalization factor is close to 1.9, falling to about 1.3 by the end of the train of 30 pulses. Thus, σ_0 is closer to σ_0^* at the end of the pulse train than at the beginning, indicating that facilitation is greater at a lower value of Ca_{ex}. This is consistent with earlier analysis (section 4.1) and analysis of the deterministic model [4]. Figure 4.1C shows the invariance property. When σ is scaled up (circles) by the $\mathcal{O}(1)$ normalization factor μ_0, the time course is almost identical to that of σ^* (solid curve). This is true over the entire stimulus train, even though σ and σ^* facilitate at two different rates and to different degrees.

The observation that the normalization factor is lower at the end of the train of pulses than at the beginning is a general result. If Ca^{2+} concentration is increased by a factor of λ, then the asymptotic value of μ_0 is obtained from (4.20) and (4.8),

$$\mu_0(\infty) = \frac{\lambda(1 + \langle\bar{c}\rangle)}{(1 + \lambda\langle\bar{c}\rangle)}. \tag{4.21}$$

Similarly, at the resting equilibrium prior to the onset of stimulation,

$$\mu_0(0) = \frac{\lambda(1 + \bar{c}(0))}{(1 + \lambda\bar{c}(0))}, \tag{4.22}$$

where $\bar{c}(0)$ is the dimensionless average domain Ca^{2+} concentration at this resting state. Since both the initial and the asymptotic normalization factors decrease monotonically with average domain Ca^{2+}, and since average domain Ca^{2+} is greater during the period of stimulation than prior to stimulation, the asymptotic normalization factor is always less than the initial factor.

While Fig. 4.1C shows invariance for a single gate, in [4] we used a Monte Carlo simulation to demonstrate invariance of release, and thus of all four gates. Indeed, the invariance property exhibited by σ_1, σ_2, and σ_3 is also exhibited by the joint expectations involving the slow gates. This is true since $\sigma_{123,0} = \sigma_{1,0}\,\sigma_{2,0}\,\sigma_{3,0}$ and thus

$$\mu_{123,0} = \mu_{1,0}(\tau)\,\mu_{2,0}(\tau)\,\mu_{3,0}(\tau). \tag{4.23}$$

An argument similar to that used in section 4.2 to show that the fast gate S_4 has no effect on facilitation can be used to show that $\mu_{j4} \approx \mu_j\,\mu_4 \approx \mu_j\,\lambda$ $(j = 1, 2, 3)$, and thus joint expectations involving the fast gate also have the invariance property. These results fully account for the invariance of release displayed by the model.

The same reasoning used to establish invariance to changes in Ca_{ex} can be used to establish a second experimentally observed invariance property. It was shown [6] that the normalized time course of facilitated release is similar to that of unfacilitated

release (although the degree of facilitation was not large). In [4] this invariance property was demonstrated using a Monte Carlo simulation. To show why this works we use the same argument as above, now letting σ^* denote the bound gate concentration during the nth stimulus (i.e., facilitated), and σ denote that during the first stimulus (unfacilitated).

4.4. Ca^{2+} cooperativity. In this section we show that the Ca^{2+} cooperativity of release is directly related to the normalization factor and thus inversely related to facilitation. The inverse relation between cooperativity and facilitation was shown by Stanley in experiments with the squid giant synapse [21] and motivated his verbal model of transmitter release which is the basis of the present mathematical model.

Cooperativity is defined as the exponent Γ such that $R \propto Ca_{ex}^{\Gamma}$, or $R \propto c^{\Gamma}$ since we assume that domain Ca^{2+} is proportional to Ca_{ex}. For each of the gates we assume a proportionality relationship between the bound gate concentration and some power of domain Ca^{2+} and define the "fractional cooperativity" as γ where $\sigma \propto c^{\gamma}$. Intuitively, the fractional cooperativity of a gate is its approximate contribution to the total cooperativity of release. In this section we obtain lower and upper bounds on the cooperativity of release and show that each gate contributes at most one to the cooperativity. We show that to leading order the cooperativity of the slow-gate subsystem is equal to the sum of the fractional cooperativities of the individual slow gates. We also show that the fast gate adds one to the total cooperativity.

For any of the four gates, if the external Ca^{2+} concentration is increased by a factor of λ, then letting σ^* correspond to higher Ca_{ex}, $\sigma^* \propto \lambda^{\gamma} c^{\gamma}$ and hence

$$\mu = \frac{\sigma^*}{\sigma} = \lambda^{\gamma}. \tag{4.24}$$

Thus, for a slow gate $\mu_0 = \lambda^{\gamma}$ to first order or

$$\gamma = \frac{\log \mu_0}{\log \lambda} \tag{4.25}$$

to first order, showing that the fractional cooperativity of this gate is no greater than one (since $\mu_0 \leq \lambda$) and, like the normalization factor μ_0, it declines slowly during a train of pulses. Furthermore, since $\mu_{123,0} = \mu_{1,0}\,\mu_{2,0}\,\mu_{3,0}$ (4.23),

$$\mu_{123,0} = \lambda^{(\gamma_1+\gamma_2+\gamma_3)} \tag{4.26}$$

to first order, and thus the cooperativity of the subsystem of slow gates is the sum of the fractional cooperativities. As discussed in section 4.3, $\mu_4 \approx \lambda$ and $\mu_{j4} \approx \mu_j\,\mu_4$ $(j = 1, 2, 3)$. The latter result is easily extended to $\mu_{1234} \approx \mu_{123}\,\mu_4$. Hence, the fast gate has fractional cooperativity $\gamma_4 = 1$ and

$$\mu_{1234} \approx \lambda^{(\gamma_1+\gamma_2+\gamma_3+1)}. \tag{4.27}$$

Now, $R^* \propto \lambda^{\Gamma} c^{\Gamma}$, so $\mu_{1234} = R^*/R = \lambda^{\Gamma}$. Hence, $\Gamma \approx \gamma_1 + \gamma_2 + \gamma_3 + 1$; i.e., the total Ca^{2+} cooperativity is approximately the sum of the four fractional cooperativities. Since the fractional cooperativity of a slow gate declines as the gate facilitates, total cooperativity also declines. Therefore, since asymptotic facilitation increases in a step-like fashion with the log of stimulus frequency, the asymptotic cooperativity of release will show a step-like *decrease* from 4 at very low stimulus frequencies to near 1 at very high frequencies, as observed experimentally [21], [23].

5. Approximations to the full model. The full model of transmitter release that we have explored in this study accounts for many features of release and facilitation. However, the simplicity of the idea behind the model, four independent sites binding Ca^{2+} at different rates and colocalized with a Ca^{2+} channel, is somewhat obscured by the large number of equations required to describe it (30 differential equations plus auxiliary equations for Ca^{2+} channel activation and voltage). In this section we discuss several approximations that can be made to reduce the number of state variables in the model, and we describe some of the qualitative and quantitative effects of these approximations.

In the first approximation we take advantage of the fast kinetics of gate S_4. Since Ca^{2+} binds (unbinds) to the gate almost immediately upon the opening (closing) of a Ca^{2+} channel, it can be assumed that the concentration of bound gates of this type is in equilibrium with the domain Ca^{2+} concentration. Thus, any differential equation involving the index 4 can be set to equilibrium, yielding a system of 16 algebraic equations that can be solved explicitly in terms of α, β, m, and Ca. With this approximation the number of differential equations is reduced to 14, but the release time course is virtually unchanged.

Another useful approximation is to include only two gates in the release site; one slow and one fast. Mean release is then determined by six differential equations, which can be reduced to two if the quasi-equilibrium assumption is made for the fast gate. This is appropriate if one requires a model of synaptic release that exhibits facilitation, but is not concerned about capturing the multiple time scales of facilitation (i.e., the facilitation steps) or the fourth-order Ca^{2+} cooperativity.

We now derive a simplification that reduces the number of differential equations to three while preserving all the features of release discussed in previous sections of the paper. It was shown in section 4.1 that for a slow gate $\sigma = \sigma_0(\tau) + \mathcal{O}(\epsilon)$, where σ_0 depends only on the time average of average domain calcium and accounts for the slow rise of σ during a train of pulses. We show now that the time course of σ during a pulse depends on the instantaneous average domain Ca^{2+} to $\mathcal{O}(\epsilon^2)$. Taken together, these results show that it is not necessary to know the detailed distribution of open Ca^{2+} channels to compute σ during a train of pulses (Fig. 5.1A).

We begin with (4.1c), which is coupled to (4.1b) by the factor σ^o. This coupling may be removed by replacing σ^o with $m\,\sigma$. Indeed,

$$\begin{aligned} \sigma^o &= \sigma_0^o + \mathcal{O}(\epsilon) \\ &= m\,\sigma_0 + \mathcal{O}(\epsilon) \\ &= m\,\sigma + \mathcal{O}(\epsilon), \end{aligned} \tag{5.1}$$

so σ should be well approximated by σ_{ADC}, a variable that depends only on average domain $Ca^{2+}$and which satisfies

$$\frac{d\sigma_{ADC}}{dt} = -\epsilon\,\sigma_{ADC} - \epsilon\,\bar{c}\,\sigma_{ADC} + \epsilon\,\bar{c}. \tag{5.2}$$

We can think of this as a "mean field" approximation: sites respond to average Ca^{2+} rather than to channel-to-channel variations in Ca^{2+}.

To analyze (5.2) we introduce the multiple scale expansion $\sigma_{ADC}(t,\tau) = \sigma_{ADC,0}\,(t,\tau) + \epsilon\,\sigma_{ADC,1}\,(t,\tau) + \epsilon^2\,\sigma_{ADC,2}\,(t,\tau) + \mathcal{O}(\epsilon^3)$ and collect terms of like powers of ϵ to obtain the $\mathcal{O}(1)$ equation

$$\frac{\partial \sigma_{ADC,0}}{\partial t} = 0, \tag{5.3}$$

which is identical to (4.2c) describing the lowest-order term in the expansion of σ. The $\mathcal{O}(\epsilon)$ equation is

$$\frac{\partial \sigma_{ADC,1}}{\partial t} = -\frac{\partial \sigma_{ADC,0}}{\partial \tau} - \sigma_{ADC,0} - \bar{c}\,\sigma_{ADC,0} + \bar{c}, \tag{5.4}$$

which is identical to the σ_1 equation (4.5). This is true because of the statistical independence property (4.3). The $\mathcal{O}(\epsilon^2)$ equation is

$$\frac{\partial \sigma_{ADC,2}}{\partial t} = -\frac{\partial \sigma_{ADC,1}}{\partial \tau} - \sigma_{ADC,1} - \bar{c}\,\sigma_{ADC,1}, \tag{5.5}$$

which differs from the $\mathcal{O}(\epsilon^2)$ equation for σ in the last term, since $\sigma_1^o \neq m\,\sigma_1$. Therefore, $\sigma_{ADC} - \sigma = \mathcal{O}(\epsilon^2)$.

A similar analysis can be carried out for gates like S_4 which are not slow (k^- not small) but for which k^+ is small, so that $k^- \gg k^+$. In this case, we use the following nondimensional form of the σ equation:

$$\frac{d\sigma}{dt} = -\kappa^-\sigma - \epsilon\, c\,\sigma^o + \epsilon\,\bar{c}, \tag{5.6}$$

where $\kappa^- = k^-\,\tau_m$, $\epsilon = k^+\,\tau_m\,K_{Ca}$, $K_{Ca} = 0.1\ \mu$M is near the resting Ca^{2+} concentration, $c = Ca\,/\,K_{Ca}$, and $\bar{c} = c\,m$. If we now introduce the regular perturbation expansion $\sigma(t) = \sigma_0(t) + \epsilon\,\sigma_1(t) + \mathcal{O}(\epsilon^2)$ and collect terms with like powers of ϵ, then we obtain the equation $d\sigma_0/dt = -\kappa^-\sigma_0$ for the $\mathcal{O}(1)$ system. Thus, σ_0 tends to 0 in $\mathcal{O}(1)$ time, contradicting the assumption that σ_0 is $\mathcal{O}(1)$. We therefore use the expansion $\sigma(t) = \epsilon\,\sigma_1(t) + \epsilon^2\,\sigma_2(t) + \mathcal{O}(\epsilon^3)$ and obtain for the $\mathcal{O}(\epsilon)$ system

$$\frac{d\sigma_1}{dt} = -\kappa^-\,\sigma_1 + \bar{c} \tag{5.7}$$

and for the $\mathcal{O}(\epsilon^2)$ system

$$\frac{d\sigma_2}{dt} = -\kappa^-\,\sigma_2 - c\,\sigma_1^o. \tag{5.8}$$

Using the same scaling as in (5.6), the nondimensional form of the equation utilizing average domain Ca^{2+} is

$$\frac{d\sigma_{ADC}}{dt} = -\kappa^-\sigma_{ADC} - \epsilon\,\bar{c}\,\sigma_{ADC} + \epsilon\,\bar{c}. \tag{5.9}$$

Introducing the expansion $\sigma_{ADC}(t) = \epsilon\,\sigma_{ADC,1}\,(t) + \epsilon^2\,\sigma_{ADC,2}\,(t) + \mathcal{O}(\epsilon^3)$, we obtain

$$\frac{d\sigma_{ADC,1}}{dt} = -\kappa^-\,\sigma_{ADC,1} + \bar{c} \tag{5.10}$$

for the $\mathcal{O}(\epsilon)$ system, and

$$\frac{d\sigma_{ADC,2}}{dt} = -\kappa^-\,\sigma_{ADC,2} - \bar{c}\,\sigma_{ADC,1} \tag{5.11}$$

for the $\mathcal{O}(\epsilon^2)$ system. Equations (5.7) and (5.10) are identical, but (5.8) and (5.11) differ since $\sigma_1^o \neq m\,\sigma_1$. Therefore, as was true for the slow gates, $\sigma_{ADC} - \sigma = \mathcal{O}(\epsilon^2)$ and the time course of σ is well approximated by σ_{ADC}.

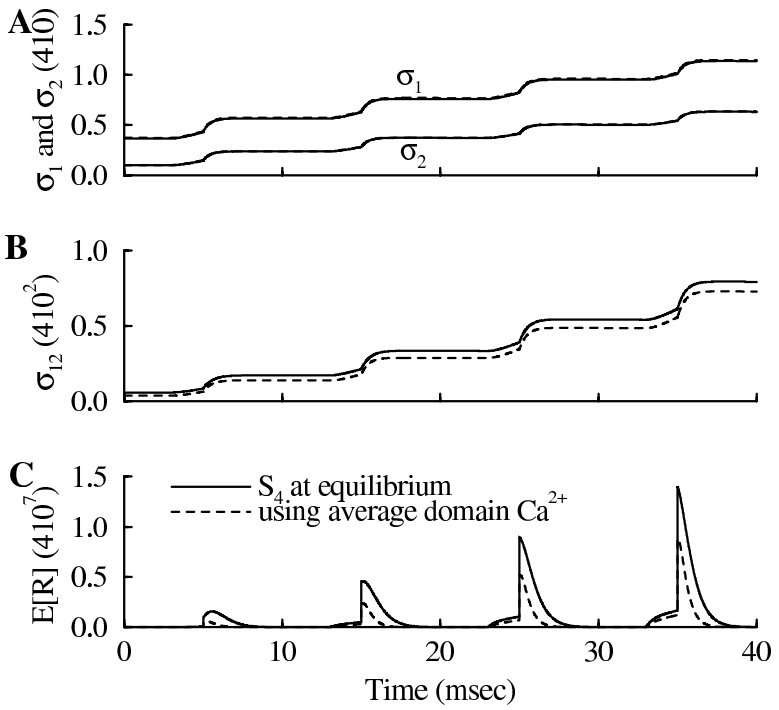

FIG. 5.1. *Release elicited by four* 2*-msec depolarizations from* −65 *mV to* 10 *mV.* (A) σ_1 *and* σ_2 *computed with* (2.11a) *and* (2.11c) *(solid) and using the average domain* Ca^{2+} *approximation* (5.2) *(dashed). The error in this approximation is* $\mathcal{O}(\epsilon^2)$. (B) σ_{12} *computed with* (2.15e) *and* (2.15f) *and as the product* $\sigma_{ADC,1}\,\sigma_{ADC,2}$. *The error in this approximation is* $\mathcal{O}(\epsilon)$. (C) *Release computed with* σ_{1234}*, but with fast equations at equilibrium (solid), and computed using the average domain* Ca^{2+} *concentration as* $\sigma_{ADC,1}\,\sigma_{ADC,2}\,\sigma_{ADC,3}\,\sigma_{ADC,4}$ *with* $\sigma_{ADC,4}$ *at equilibrium (dashed).* $Ca_{ex} = 1$ *mM.*

We now relate these results to release. In terms of dimensional parameters and variables,

$$\frac{d\sigma_{ADC,j}}{dt} = k_j^+\,\overline{Ca} - (k_j^- + k_j^+\,\overline{Ca})\,\sigma_{ADC,j}, \tag{5.12}$$

where $j = 1,2,3,4$ now denotes gate type rather than power of ϵ and where $\overline{Ca} = mCa$. In section 4.2 we showed that $\sigma_{123} = \sigma_1\,\sigma_2\,\sigma_3 + \mathcal{O}(\epsilon)$. This remains $\mathcal{O}(\epsilon)$ accurate if σ_j is replaced by $\sigma_{ADC,j}$. A more careful multiple scale analysis with three time scales (unpublished) shows that

$$E[R] = \sigma_{ADC,1}\,\sigma_{ADC,2}\,\sigma_{ADC,3}\,\sigma_{ADC,4} + \mathcal{O}(\epsilon). \tag{5.13}$$

This reduces the number of differential equations to four or three if $\sigma_{ADC,4}$ is taken to equilibrium, plus auxiliary equations. In Fig. 5.1 we see that the errors in the approximations to σ_1 and σ_2 are small ($\mathcal{O}(\epsilon^2)$) (Fig. 5.1), the error in the approximation to the joint expectation σ_{12} is larger ($\mathcal{O}(\epsilon)$) (Fig. 5.1B), and the error in the approximation to release is larger still (Fig. 5.1C). However, the simplicity of this form of the model makes the error acceptable for many applications.

Finally, in the limiting case of instantaneous channel kinetics, which means that $\epsilon = k^-\,\tau_m \to 0$, scheme (5.13) reduces to the deterministic model of section 2.1. If

stimulation is through voltage clamp steps, which means that V and Ca are piecewise constant, then an analytical expression can be obtained for release [4], bringing us full circle back to the simple, intuitive picture we began with in [4]. The deterministic model retains many of the properties of the stochastic model and of experiment [4] and may be appropriate in simulations of large networks of interconnected neurons, particularly where membrane potential is not an explicit state variable (see [3]).

6. Concluding remarks. We developed a simple method for representing the collective effect of a population of colocalized release sites and stochastic Ca^{2+} channels without direct Monte Carlo simulation. We first reformulated the stochastic problem as a system of hyperbolic conservation equations for the probability distributions of bound gates and then used these to derive differential equations for the mean concentrations of bound gates and for the mean rate of release. Using a multiple scale analysis we uncovered several properties of release that are consistent with experimental data. These include facilitation of release that decreases with the external Ca^{2+} concentration; a step-like frequency dependence of facilitation; Ca^{2+} cooperativity that declines in a step-like manner with facilitation; and a release time course that is invariant to changes in the magnitude of release, whether due to facilitation or to changes in external Ca^{2+}. Also as a result of this analysis, we established that release computed with the average domain Ca^{2+} concentration is a good approximation to release computed using the detailed distribution of open Ca^{2+} channels. This greatly simplifies the model, so that mean release can be computed with just three differential equations. This and other suggested reduced forms makes the model sufficiently simple for use with models of neuronal electrical activity or with networks of model neurons. For example, by coupling the release model to a model of dopamine-secreting neurons [14], we have shown that transmitter release is greater when the neuron bursts than when it spikes continuously [3].

Our model of release differs from two of the best-known models [17], [24] in several ways. In both [17] and [24], facilitation is due primarily to residual-free Ca^{2+}, although [24] does include a slow Ca^{2+} binding site in the release mechanism. Neither [17] nor [24] is able to account for the step-like frequency dependence reported in [21]. One model, [17], was developed to explain the apparent time course invariance to changes in the magnitude of release. This was achieved by postulating that the release time course is determined by the membrane voltage, rather than by the local Ca^{2+} concentration. Since voltage is unaffected by facilitation or changes in the external Ca^{2+} concentration, this approach captures the time course invariance. However, there is considerable evidence against such a role for voltage [27], [13]. In the present paper we have shown that invariance in the release time course to changes in the magnitude of release is a robust feature of our model, although it does begin to break down at very high (and probably unphysiological) Ca^{2+} concentrations. Thus, our model has the invariance properties described in [6] and yet has a time course dependent only on Ca^{2+} and the kinetics of Ca^{2+} binding and unbinding.

We have made several simplifications and assumptions in the model. We have assumed that no more than one channel is open at a time at a given release site and that Ca^{2+} from other open channels does not reach this site. These assumptions allow us to neglect Ca^{2+} diffusion, but we expect them to be valid only when release is evoked by brief depolarizations, such as action potentials. We have also assumed that Ca^{2+} influx is proportional to the external Ca^{2+} concentration, thus neglecting

the effect of Ca^{2+} at the inner mouth of the channel on the concentration gradient across the channel. This assumption is not crucial to our results, as they can be reproduced [4] using values of Ca^{2+} concentration from a simulation of three-dimensional diffusion near an open channel that takes this effect into consideration [1]. Finally, we have assumed that the vesicle pool is inexhaustible and the release sites do not inactivate.

The structure of the vesicle docking site is presently unknown, although there is general agreement that it contains at least four Ca^{2+} binding sites. In our model we have assumed that there are four physically independent binding sites, but the actual binding process could be different. For example, the sites could be sequentially linked and noncooperative [10] or they could be cooperative such that when Ca^{2+} binds to one site the affinities of the others change [9]. The analysis presented here is not limited to physically independent sites; it is equally applicable to any binding scheme gated by Ca^{2+}.

Finally, although the object of our analysis is a model of transmitter release with colocalized Ca^{2+} channels and release sites, it applies equally well to any system of colocalized ion channels and ion receptors. For example, one class of potassium channels is known to be coactivated by Ca^{2+} and voltage. It is now thought that these channels have multiple Ca^{2+} binding sites and are colocalized with Ca^{2+} channels [12], [20]. As another example, Ca^{2+} channels that are activated by inositol 1,4,5-trisphosphate (IP_3) are present on the membrane of the endoplasmic reticulum in many cells. These channels are coactivated by Ca^{2+} and *inactivated* by Ca^{2+} on a slower time scale. This is clearly an instance where the Ca^{2+} channel and Ca^{2+} binding site (the inactivation site) are colocalized.

Appendix A. Membrane potential and domain Ca^{2+}. We assume that Ca^{2+} concentration in the domain surrounding the mouth of an open channel is proportional to the Ca^{2+} current through the channel. For the single-channel current we use the Goldman–Hodgkin–Katz formula [8], neglecting the effect of intracellular Ca^{2+} at the inner mouth of the channel:

$$i(V) = \hat{g}_{Ca} P \frac{2FV}{RT} \left[\frac{Ca_{ex}}{1 - \exp(2FV/RT)} \right]. \tag{A.1}$$

Here $\hat{g}_{Ca}$ is the single-channel conductance, P converts concentration to membrane potential, Ca_{ex} is the external Ca^{2+} concentration, and RT/F is the thermal voltage (26.7 mV). We use $\hat{g}_{Ca} = 12$ pS and $P = 1.6$ mV mM^{-1}. Domain Ca^{2+} concentration is then $Ca = -A\, i(V)$, where we use the value $A = 0.1$ μM fA^{-1}, and the negative sign is introduced since the current is negative.

The voltage-dependent Ca^{2+} channel opening rate, $\alpha = 0.6\, e^{V/10}$, and closing rate, $\beta = 0.2\, e^{-V/26.7}$, are based upon measurements from the squid giant synapse [15].

In Fig. 3.1, asymptotic facilitation from a long train of action potentials is computed numerically. We use the Hodgkin–Huxley equations to generate an action potential [11]:

$$C_m \frac{dV}{dt} = -[\bar{g}_{Na}\, x^3\, h\, (V - V_{Na}) + \bar{g}_K\, n^4\, (V - V_K) + \bar{g}_{leak}\, (V - V_{leak}) - I_{app}], \tag{A.2a}$$

$$\frac{dx}{dt} = (x_\infty(V) - x)/\tau_x(V), \tag{A.2b}$$

$$\frac{dn}{dt} = (n_\infty(V) - n)/\tau_n(V), \tag{A.2c}$$

$$\frac{dh}{dt} = (h_\infty(V) - h)/\tau_h(V), \tag{A.2d}$$

where $x_\infty(V) = \alpha_x/(\alpha_x+\beta_x)$, $\tau_x(V) = 1/(\alpha_x+\beta_x)$ (similarly for n_∞, h_∞, τ_n, and τ_h) and $\alpha_x = 0.1(V+40)/[1-e^{-(V+40)/10}]$, $\beta_x = 4\,e^{-(V+65)/18}$, $\alpha_n = 0.01(V+55)/[1-e^{-(V+55)/10}]$, $\beta_n = 0.125\,e^{-(V+65)/80}$, $\alpha_h = 0.07\,e^{-(V+65)/20}$, $\beta_h = 1/[1+e^{-(V+35)/10}]$. Here x, n, and h are gating variables, C_m is the membrane capacitance, $\bar{g}_{Na}$, $\bar{g}_K$, $\bar{g}_{leak}$ are the maximum conductances for the sodium, potassium, and leak currents, and V_{Na}, V_K, and V_{leak} are the corresponding reversal potentials. Parameter values are $C_m = 1\ \mu\mathrm{F\,cm^{-2}}$, $\bar{g}_{Na} = 120\ \mathrm{mS\,cm^{-2}}$, $\bar{g}_K = 36\ \mathrm{mS\,cm^{-2}}$, $\bar{g}_{leak} = 0.3\ \mathrm{mS\,cm^{-2}}$, $V_{Na} = 50$ mV, $V_K = -77$ mV, and $V_{leak} = -54$ mV. To induce an action potential a depolarizing current of $I_{app} = 30\ \mu\mathrm{A\,cm^{-2}}$ is applied for 2 msec. Consistent with experimental data [15], [21], we assume that the contribution made by Ca^{2+} current to the membrane potential is small, and we omit it from the voltage equation.

Appendix B. Numerical integration of the hyperbolic equations. A first-order upwind differencing scheme [18] is used to numerically integrate (2.5a) and (2.5b). Application of the scheme to (2.5a) is standard since the characteristics all contract leftward toward $u = 0$ (Fig. 2.2). The characteristics of (2.5b) contract toward $u = \bar{u}$, so the differencing stencil on the left of $\bar{u}$ is different from that on the right. Furthermore, $\bar{u}$ is voltage dependent, so that the interval over which each stencil is applied changes with time and must be determined at each time step.

This differencing scheme captures the transport nature of the equations but does not conserve mass. Thus, the p_0 and p_1 populations are renormalized at each time step. The extended trapezoidal rule [18] is used to obtain approximations A_1 and A_0 of $\int_0^1 p_1(u,t)\,du$ and $\int_0^1 p_0(u,t)\,du$, respectively. Then at each grid point, u_i, we multiply $p_1(u_i,t)$ by the ratio m/A_1, and $p_0(u_i,t)$ by the ratio $(1-m)/A_0$. Initial conditions must be specified so that $A_1 = m$ and $A_0 = 1-m$ at the start of the simulation.

Appendix C. Derivation of the equations for mean release assuming both channels and gates are stochastic. The equations for mean release (2.11a), (2.11b), (2.15a)–(2.15f) can be derived from the balance equations for the complete set of release site configurations. To demonstrate how this is done we consider release sites with two gates and an associated Ca^{2+} channel. A schematic diagram of the gating kinetics is shown in Fig. C.1. The state of a release site associated with an open (closed) Ca^{2+} channel is denoted by S^o_{ij} (S^c_{ij}), where i represents the first gate and j represents the second gate. If a gate is bound then the index equals 1, otherwise it equals 0. For example, S^c_{10} denotes a release site with the first gate occupied and the second gate unoccupied. The associated Ca^{2+} channel is closed. For simplicity, we also let S^c_{10} denote the probability that the release site is in this state.

The sum of the states on the back (front) face of the box in Fig. C.1 is equal to the probability that a Ca^{2+} channel is open (closed),

$$\sum_{i,j} S^o_{ij} = m, \tag{C.1}$$

$$\sum_{i,j} S^c_{ij} = 1 - m. \tag{C.2}$$

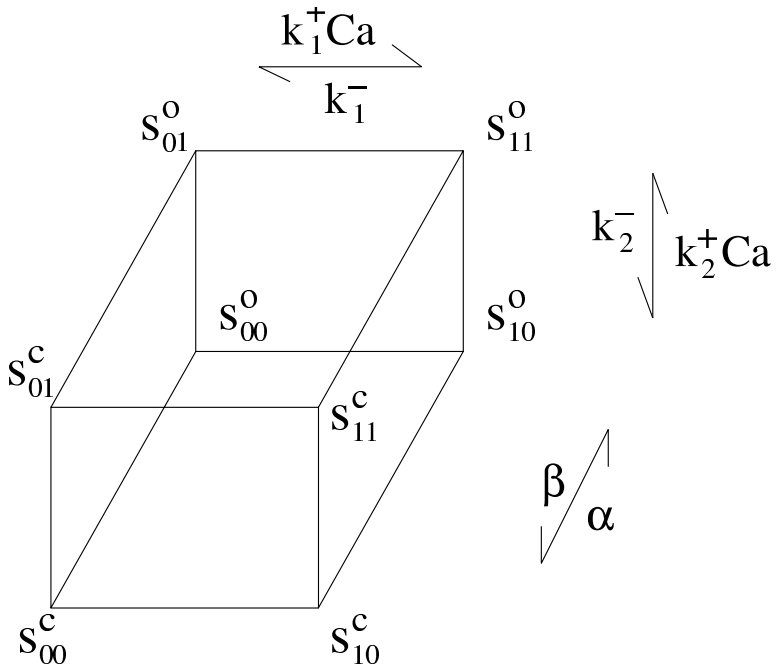

FIG. C.1. *Schematic diagram of the gating kinetics for a release site with two gates and a* Ca^{2+} *channel with a single open and a single closed state. The eight corners of the box represent the eight possible configurations of the gate/channel complex. Each corner also represents a probability, and the sum of the probabilities is* 1. *The gate binding/unbinding rates and channel open/closed rates are indicated next to the kinetic diagram. On the front face* $Ca = 0$, *so only downward and leftward transitions are possible.*

The evolution equations for the different configuration probabilities are determined from the gating kinetics. For example,

$$\frac{dS^c_{10}}{dt} = k_2^- \, S^c_{11} \, + \, \beta \, S^o_{10} \, - \, (k_1^- \, + \, \alpha) \, S^c_{10}. \tag{C.3}$$

The evolution of all release site configurations is described by six differential equations along with the two conservation equations (C.1), (C.2).

There is a simple linear transformation from the configuration variables to the σ variables used throughout the text. For example, σ_1^o is the probability that the first gate is bound and the associated Ca^{2+} channel is open; thus $\sigma_1^o = S^o_{10} + S^o_{11}$. For release sites with two gates, the complete set of transformations is

$$\sigma^c_{12} = S^c_{11}, \;\; \sigma^c_1 = S^c_{10} + S^c_{11}, \;\; \sigma^c_2 = S^c_{01} + S^c_{11}, \tag{C.4}$$

$$\sigma^o_{12} = S^o_{11}, \;\; \sigma^o_1 = S^o_{10} + S^o_{11}, \;\; \sigma^o_2 = S^o_{01} + S^o_{11}. \tag{C.5}$$

Applying these transformations in the release site configuration equations, one arrives at the σ equations for release sites with two gates.

Acknowledgments. The authors thank Bard Ermentrout for suggesting the use of conservation equations and both Bard Ermentrout and Mark Pernarowski for helpful comments on the multiple scale analysis. Much of this work was performed while Richard Bertram was at the Mathematical Research Branch, NIDDK, NIH.

REFERENCES

[1] S. Aharon, H. Parnas, and I. Parnas, *The magnitude and significance of Ca^{2+} domains for release of neurotransmitter*, Bull. Math. Biol., 56 (1994), pp. 1095–1119.

[2] G. J. Augustine, E. M. Adler, and M. P. Charlton, *The calcium signal for transmitter secretion from presynaptic nerve terminals*, Ann. New York Acad. Sci., 635 (1991), pp. 365–381.

[3] R. Bertram, *A simple model of transmitter release and facilitation*, Neural Computation, 9 (1997), pp. 515–523.

[4] R. Bertram, A. Sherman, and E. F. Stanley, *Single-domain/bound calcium hypothesis of transmitter release and facilitation*, J. Neurophysiol., 75 (1996), pp. 1919–1931.

[5] R. D. Burgoyne and A. Morgan, *Ca^{2+} and secretory-vesicle dynamics*, Trends Neurosci., 18 (1995), pp. 191–196.

[6] N. B. Datyner and P. W. Gage, *Phasic secretion of acetylcholine at a mammalian neuromuscular junction*, J. Physiol. (Lond.), 303 (1980), pp. 299–314.

[7] R. F. Fox and Y.-N. Lu, *Emergent collective behavior in large numbers of globally coupled independently stochastic ion channels*, Phys. Rev. E, 49 (1994), pp. 3421–3431.

[8] D. E. Goldman, *Potential, impedance, and rectifications in membranes*, J. Gen. Physiol., 27 (1943), pp. 36–60.

[9] R. Heidelberger, C. Heinemann, E. Neher, and G. Matthews, *Calcium dependence of the rate of exocytosis in a synaptic terminal*, Nature, 371 (1994), pp. 513–515.

[10] C. Heinemann, R. H. Chow, E. Neher, and R. S. Zucker, *Kinetics of the secretory response in bovine chromaffin cells following flash photolysis of caged Ca^{2+}*, Biophys. J., 67 (1994), pp. 2546–2557.

[11] A. L. Hodgkin and A. F. Huxley, *A quantitative description of membrane current and its application to conduction and excitation in nerve*, J. Physiol. (Lond.), 117 (1952), pp. 500–544.

[12] A. J. Hudspeth and R. S. Lewis, *Kinetic analysis of voltage- and ion-dependent conductances in saccular hair cells of the bull-frog, Rana catesbeiana*, J. Physiol. (Lond.), 400 (1988), pp. 237–274.

[13] L. Landò and R. S. Zucker, *Ca^{2+} cooperativity in neurosecretion measured using photolabile Ca^{2+} chelators*, J. Neurophysiol., 72 (1994), pp. 825–830.

[14] Y.-X. Li, R. Bertram, and J. Rinzel, *Modeling N-methyl-D-aspartate-induced bursting in dopamine neurons*, Neuroscience, 71 (1996), pp. 397–410.

[15] R. Llinás, I. Z. Steinberg, and K. Walton, *Presynaptic calcium currents in squid giant synapse*, Biophys. J., 33 (1981), pp. 289–322.

[16] R. Llinás, I. Z. Steinberg, and K. Walton, *Relationship between presynaptic calcium current and postsynaptic potential in squid giant synapse*, Biophys. J., 33 (1981), pp. 323–352.

[17] H. Parnas, J. Dudel, and I. Parnas, *Neurotransmitter release and its facilitation in the crayfish. VII. Another voltage dependent process besides Ca entry controls the time course of phasic release*, Pflügers Arch., 406 (1986), pp. 121–130.

[18] W. H. Press, B. P. Flannery, S. A. Teukolsky, and W. T. Vetterling, *Numerical Recipes: The Art of Scientific Computing*, Cambridge University Press, Cambridge, 1987.

[19] R. Rahamimoff, *A dual effect of calcium ions on neuromuscular facilitation*, J. Physiol. (Lond.), 195 (1968), pp. 471–480.

[20] W. M. Roberts, R. A. Jacobs, and A. J. Hudspeth, *Colocalization of ion channels involved in frequency selectivity and synaptic transmission at presynaptic active zones of hair cells*, J. Neurosci., 10 (1990), pp. 3664–3684.

[21] E. F. Stanley, *Decline in calcium cooperativity as the basis of facilitation at the squid giant synapse*, J. Neurosci., 6 (1986), pp. 782–789.

[22] E. F. Stanley, *Single calcium channels and acetylcholine release at a presynaptic nerve terminal*, Neuron, 11 (1993), pp. 1007–1011.

[23] E. F. Stanley, *Calcium binding sites of the transmitter release mechanism: Clues from short-term facilitation*, J. Physiol. (Paris), 89 (1995), pp. 163–166.

[24] W. M. Yamada and R. S. Zucker, *Time course of transmitter release calculated from simulations of a calcium diffusion model*, Biophys. J., 61 (1992), pp. 671–682.

[25] D. Yoshikami, Z. Bagaboldo, and B. M. Olivera, *The inhibitory effects of omega-conotoxins on Ca channels and synapses*, Ann. N. Y. Acad. Sci., 560 (1989), pp. 230–248.

[26] R. S. Zucker and A. L. Fogelson, *Relationship between transmitter release and presynaptic calcium influx when calcium enters through discrete channels*, Proc. Natl. Acad. Sci. USA, 83 (1986), pp. 3032–3036.

[27] R. S. Zucker and L. Landò, *Mechanism of transmitter release: Voltage hypothesis and calcium hypothesis*, Science, 231 (1986), pp. 574–579.